

Invited Research Article

Upper Permian to lowermost Triassic carbon isotope stratigraphy of Iranian open-marine successions

Sakineh Arefifard^{a*}, Christoph Korte^b, Jonathan L. Payne^c^a Department of Geology, Lorestan University, Khorramabad, Lorestan 68151-44316, Iran^b Department of Geosciences and Natural Resource Management, University of Copenhagen, 1350 Copenhagen, Denmark^c Department of Earth and Planetary Sciences, Stanford University, Stanford, California, USA

ARTICLE INFO

Editor: Prof. S Shen

Keywords:
Upper Permian
Carbon cycle
Iran
deep-water successions
diagenesis

ABSTRACT

The end-Permian mass extinction is widely interpreted to have occurred in response to a carbon cycle perturbation and its environmental consequences. However, the distinctiveness of the boundary event relative to the long-term background variations remains incompletely resolved. Variations of both $\delta^{13}\text{C}_{\text{carb}}$ and $\delta^{13}\text{C}_{\text{org}}$ have been reported in some Lopingian (Upper Permian) stratigraphic sections, but the extent to which they represent global carbon cycle dynamics remains uncertain. The paucity of carbon-isotope records for the Upper Permian creates challenges for interpreting the boundary event within its long-term context. In this study, we report new marine $\delta^{13}\text{C}_{\text{carb}}$ and $\delta^{13}\text{C}_{\text{org}}$ data from Lopingian and lowermost Triassic successions in the Ali Bashi and Zal sections, Julfa region, NW Iran, and two sections in Hambast Valley, Abadeh region, SW Iran as well as using data from Korte et al. (2004a) representing a third section in Abadeh. We also compare these new data with existing records from other deep-water Permian-Triassic (P-Tr) sections in South China. In most of those P-Tr sections, there is substantial correspondence between $\delta^{13}\text{C}_{\text{carb}}$ and $\delta^{13}\text{C}_{\text{org}}$ across the P-Tr boundary, confirming prior interpretations that the negative excursion in $\delta^{13}\text{C}_{\text{carb}}$ and $\delta^{13}\text{C}_{\text{org}}$ records a global carbon cycle perturbation. On the other hand, $\delta^{13}\text{C}_{\text{carb}}$ records from Upper Permian (Wuchiapingian and Changhsingian) deep-water sections in Iran and South China exhibit conflicting stratigraphic variation, likely due to the local influences of meteoric and/or burial diagenesis. The lack of reproducibility between Iranian and Chinese sections of the Upper Permian $\delta^{13}\text{C}_{\text{carb}}$ and $\delta^{13}\text{C}_{\text{org}}$ shifts and evidence for diagenetic alteration highlights the challenges of interpreting carbon cycle dynamics from the geological past without multiple tests, such as correlation across space and correspondence of $\delta^{13}\text{C}_{\text{carb}}$ and $\delta^{13}\text{C}_{\text{org}}$ records. The new data from the Julfa and Abadeh sections add to the evidence that the Late Permian carbon cycle was generally stable for millions of years prior to the end-Permian carbon isotope excursion and associated mass extinction event.

1. Introduction

The biological devastation of the end-Permian mass extinction (EPME) (Erwin, 2006; Shen et al., 2011; Payne and Clapham, 2012) is closely associated with evidence of environmental changes recorded in isotope proxy records of carbon, oxygen, sulfur, nitrogen, and uranium, among other elements (e.g., Korte et al., 2004a; Luo et al., 2011; Brennecka et al., 2011; Sun et al., 2012; Joachimski et al., 2012; Romano et al., 2013; Schobben et al., 2015; Lau et al., 2016; Elrick et al., 2017; Bernasconi et al., 2017; Zhang et al., 2018; Sial et al., 2021). Among these, the carbon-isotope record is the most intensively studied. A negative shift by $\sim 5\text{‰}$ in the carbon isotope composition of marine

carbonate sediments has been recorded in numerous sections spanning Armenia (Baud et al., 1989; Zakharov et al., 2005; Joachimski et al., 2020), Austria (Holser et al., 1989), South China (Xu and Yan, 1993; Jin et al., 2000; Cao et al., 2002; Nan and Liu, 2004; Krull et al., 2004; Payne et al., 2004; Shen et al., 2013), Iran (Heydari et al., 2000, 2001, 2003; Korte et al., 2004a; Korte and Kozur, 2005; Horacek et al., 2007a; Shen et al., 2013; Schobben et al., 2014), Pakistan (Baud et al., 1996; Korte et al., 2010; Brookfield et al., 2022), Italy (Magaritz et al., 1988; Korte and Kozur, 2005; Horacek et al., 2007b; Jurikova et al., 2020), Oman (Richoz, 2006; Richoz et al., 2010), and Japan (Musashi et al., 2001; Horacek et al., 2009), among others reviewed in Korte and Kozur (2010).

* Corresponding author.

E-mail address: arefi.s@lu.ac.ir (S. Arefifard).

The carbon-isotope ratio of organic matter ($\delta^{13}\text{C}_{\text{org}}$) also shifts toward lighter values across the Permian-Triassic (P-Tr) boundary in many sections (Wignall et al., 1998; Cao et al., 2002; Luo et al., 2014; Hermann et al., 2010; Algeo et al., 2012; Sanson-Barrera et al., 2015; Brookfield et al., 2018). Although the changes in the carbon-isotope record are well documented, the causes of these shifts and their implications for P-Tr environmental conditions remain debated. Many prior studies have assumed or argued that $\delta^{13}\text{C}_{\text{carb}}$ variations at the P-Tr transition reliably record a perturbation to the global carbon cycle and associated change in the isotope composition of marine dissolved inorganic carbon (DIC) (Payne et al., 2004; Korte and Kozur, 2010; Shen et al., 2013; Saitoh and Isozaki, 2021). However, others have argued that the geochemical signals of P-Tr samples are diagenetically altered, at least in part, and that the $\delta^{13}\text{C}_{\text{carb}}$ records of these samples do not reliably record variation of isotopic composition of marine DIC (Heydari et al., 2001; Schobben et al., 2016; Li, 2017). Correspondence between $\delta^{13}\text{C}_{\text{carb}}$ and $\delta^{13}\text{C}_{\text{org}}$ records has often been used as evidence of a primary signal because carbonates and organic matter are not altered by the same processes; therefore, diagenetic processes should remove any covariation and are highly unlikely to introduce it. Covariation between $\delta^{13}\text{C}_{\text{carb}}$ and $\delta^{13}\text{C}_{\text{org}}$ values, showing a parallel decline, occurs in P-Tr boundary successions in Italy (Sephton et al., 2002), Kashmir (Algeo et al., 2007), Austria (Magaritz et al., 1992), and mid-Panthalassa (Musashi et al., 2001), but diverging trends are present in sections from Japan (Takahashi et al., 2010), South China (Cao et al., 2002; Riccardi et al., 2007; Saitoh and Isozaki, 2021), Arctic Canada (Algeo et al., 2012), and Iran (Korte et al., 2004a).

In contrast to the numerous P-Tr boundary records, there are relatively few detailed and continuous carbon-isotope records spanning the entire Upper Permian. The most complete Upper Permian carbon-isotope records all derive from south China and yield mutually contradictory patterns. The Meishan section exhibits isotopic stability, with relatively heavy $\delta^{13}\text{C}_{\text{carb}}$ values up to the end-Permian extinction event (EPME) whereas the Shangsi (Shen et al., 2013) and Chaotian (Saitoh and Isozaki, 2021) sections each exhibit a protracted, negative $\delta^{13}\text{C}_{\text{carb}}$ excursion prior to the well-known excursion associated with the EPME. Consequently, the extent to which the end-Permian carbon-cycle perturbation was a departure from Late Permian background conditions remains incompletely understood due to both contradictory signals and lack of paleogeographic spread in available data.

Iran contains several stratigraphic sections that are important, or potentially important, for understanding Late Permian carbon-cycle dynamics leading up to and through the P-Tr boundary event because these successions are: a) stratigraphically expanded and relatively complete; b) biostratigraphically well constrained by conodonts and ammonites as well as foraminifers; and c) deposited at or near the paleoequator. In particular, these characteristics apply to sections from Julfa, NW Iran (e.g. Stepanov et al., 1969; Teichert et al., 1973; Baud et al., 1989; Korte and Kozur, 2005; Leda et al., 2014; Ghaderi et al., 2014a, 2014b; Ghaderi et al., 2016; Ghaderi et al., 2019; Schobben et al., 2014, 2015; Korn et al., 2016; Korn and Ghaderi, 2019; Korn and Ghaderi, 2019; Gliwa et al., 2020, 2021, 2022; Spina et al., 2020; Niko and Badpa, 2021; Hemmati et al., 2024) and Abadeh, SW Iran (e.g. Kozur, 1975, Kozur, 1977; Taraz et al., 1981; Kozur, 2007; Heydari et al., 2001; Heydari et al., 2008; Korte et al., 2004a; Korte and Kozur, 2010; Liu et al., 2013; Chen et al., 2020; Korn et al., 2021a,b; Viaretti et al., 2021; Baud et al., 2021). Korn et al. (2021a,b) presented new Changhsingian ammonoid zonations for the Baghuk section not for the Abadeh sections.

Prior research on Iranian P-Tr successions has concentrated on the P-Tr boundary and the strata immediately below and above the extinction horizon. By contrast, the long-term records of carbonate and organic carbon isotope trends for Iranian successions are rare, incomplete, or at low resolution (e.g. Heydari et al., 2000, 2001; Korte et al., 2004a, 2004b; Korte and Kozur, 2010; Korte and Kozur, 2005; Richoz, 2006; Richoz et al., 2010; Liu et al., 2013; Schobben et al., 2014; Schobben et al., 2017; Schobben et al., 2018) and, moreover, do not span the entire

Lopingian despite the fact that exposed strata extend through much of the Upper Permian and Lower Triassic. Long-term carbon isotope records are essential for understanding the Permian-Triassic biotic events, offering valuable insights into the environmental and ecological processes that drove the dramatic Earth-system changes at this time. They serve as a key tool for examining the catastrophic changes at the Permian-Triassic boundary, connecting massive carbon releases to climate shifts, changes in ocean chemistry, and the resulting mass extinction. These records are fundamental for uncovering the causes, impacts, and feedback mechanisms behind the most severe crisis in Earth's history. In prior work, Shen et al. (2013) recognized that the Upper Permian stratigraphic sections and carbon isotope records from China and Iran are among the most complete in the world. Within each region, there are differences in the carbon-isotope patterns that raise questions about which, if any, best represents variation in the global pool of dissolved inorganic carbon (DIC). However, the Iranian sections remain less studied than the Chinese sections and further effort is required to assess which aspects of the signal are shared between China and Iran as well as which variations reflect global versus local processes.

To address this gap in knowledge, here we present the first continuous, paired $\delta^{13}\text{C}_{\text{carb}}$ and $\delta^{13}\text{C}_{\text{org}}$ records for deeper-water Upper Permian (Wuchiapingian and Changhsingian) to shallow-water, lowermost Triassic deposits in both the Ali Bashi and the Zal sections in the Julfa region, NW Iran (Fig. 1). We also present Upper Permian to lowermost Triassic carbon- and oxygen-isotope records from two sections in the Hambast Valley of the Abadeh region, SW Iran, here called the Abadeh-1 and Abadeh-2 sections, as well as $\delta^{13}\text{C}_{\text{org}}$ data reported in Korte et al. (2004a), herein termed the Abadeh-3 section, which is close to our Abadeh-1 section. This additional section was originally reported by Korte et al. (2004a). The new data set presented in the present study enables detailed carbon-isotope ($\delta^{13}\text{C}_{\text{carb}}$ and $\delta^{13}\text{C}_{\text{org}}$) stratigraphy of this interval for Iran. Additionally, it provides an opportunity to compare the new results for both carbonates and organic matter from Iran with previously reported $\delta^{13}\text{C}_{\text{carb}}$ and $\delta^{13}\text{C}_{\text{org}}$ records from South China to reassess the extent to which variations result from global carbon cycle dynamics versus local syn- and/or post-depositional processes.

2. Geologic setting

In total, five Upper Permian to Lower Triassic sections in Julfa and Abadeh were investigated in the present study (Fig. 1). The sections in Julfa are Ali Bashi (in the Ali Bashi Mountains, 9 km west of Julfa, NW Iran, the location of the Ali Bashi section in this study is very close to Locality 4 of Teichert et al. (1973), coordinates for the base of the section: N38°56'27.6", E045°30'42.8") and Zal (in the Zal Mountains, 22 km SSW of Julfa and 2.4 km NW of Zal village, coordinates for the base of the section: N38°43'58.4", E045°34'41.7") and for Abadeh are Abadeh-1 (in southeast flank of main Hambast Valley, about 35 km southeast of Abarkuh and about 60 km of southeast of Abadeh, coordinates for the base of the section: N 30°54'01.5", E 53°12'34.3"), Abadeh-2 (about 200 m beyond the entrance of the Hambast Valley and ca. 2 km northwest of the first section, coordinates for the base of the section: N 30°55'04.8", E 53°12'14.5) and Abadeh-3 (Fig. 1). The latter, located close to the Abadeh-1 section, was described by Korte et al. (2004a). The Julfa area is part of the Alborz block situated in the western side of the Alborz Mountains (Alavi, 1991, 1996). The Paleozoic successions in the Julfa area resemble those in the Alborz block; however, the Julfa area experienced more continuous deposition during the Late Permian and P-Tr transition due to tectonic subsidence, despite sea-level fall and in contrast to laterization in most parts of the Alborz block.

The Abadeh area is on the western side of the Central Iran Micro-continent and is part of the Sanandaj-Sirjan Structural Zone (Alavi, 1991, 1996; Aghanabati, 2004). The Sanandaj-Sirjan Zone is located northeast of the Neo-Tethys suture and along the Main Zagros thrust (MZT) within the Zagros Mountains (Stampfli and Borel, 2002). Using tectonic subsidence curves in Alborz and Abadeh, Hassanzadeh and

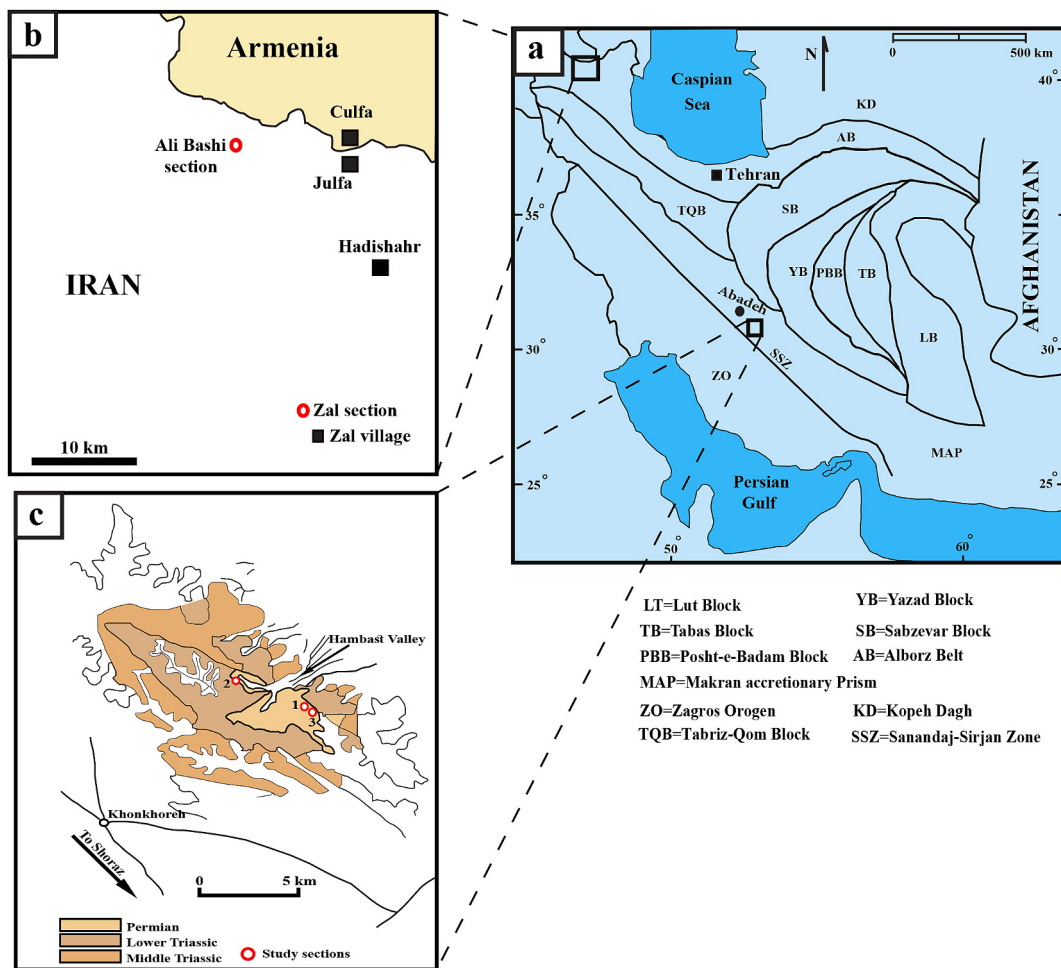


Fig. 1. (a) Generalized tectonic map of Iran (adapted from Alavi, 1991), (b) index map (adapted from Leda et al., 2014) showing the locations of Ali Bashi and Zal section in Julfa region, NW of Iran, and (c) generalized geologic map of region (adapted from Heydari et al., 2000) illustrating the localities of the Abadeh-1, 2 and 3 sections, in Hambast Valley, Abadeh region, SW of Iran.

Wernicke (2016) concluded that there is a thickening of Upper Permian-Lower Triassic successions from northern Iran toward Abadeh, indicative of increasing subsidence rates to the south.

3. Lithostratigraphy

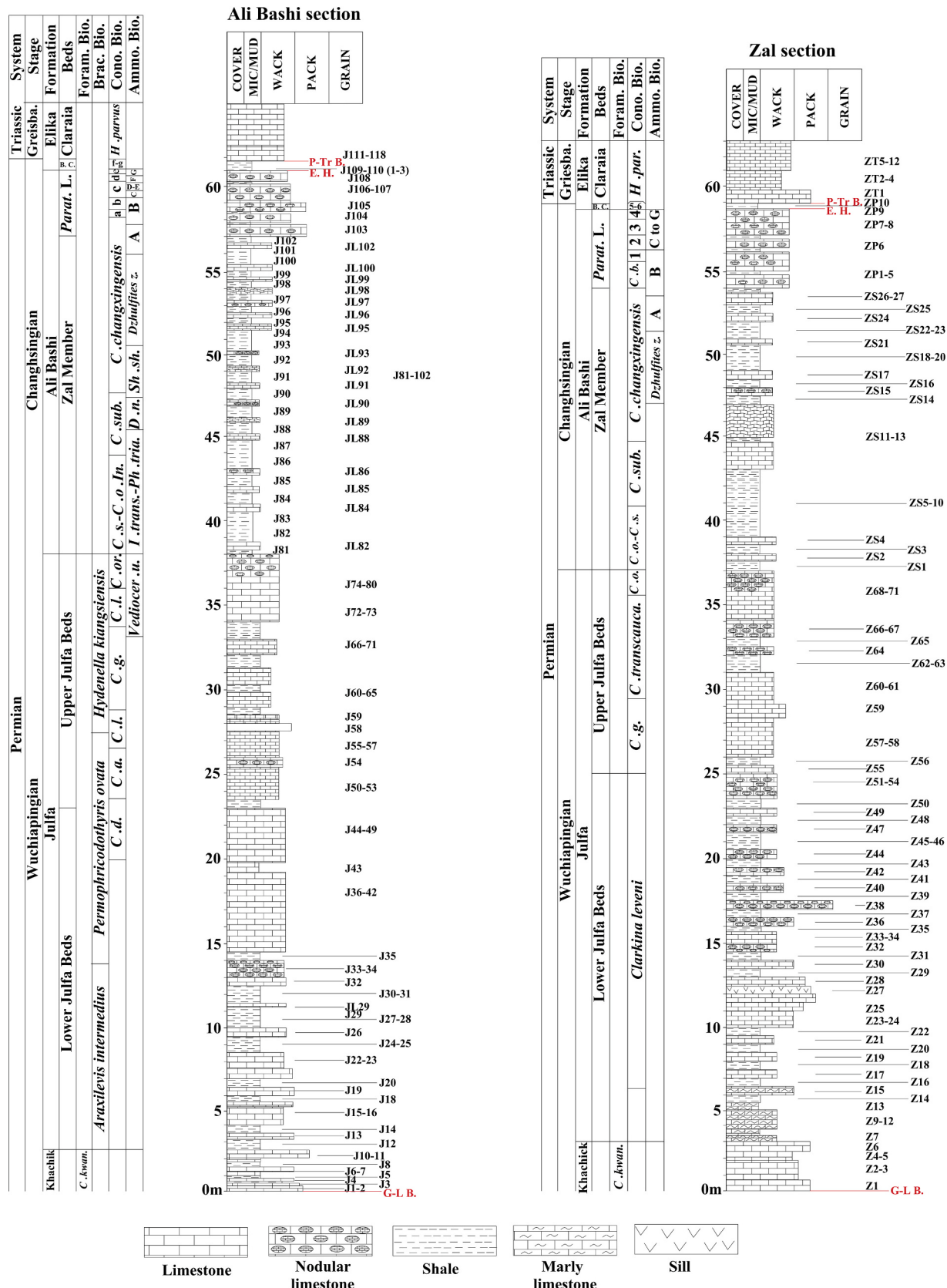
3.1. Lithostratigraphy of Ali Bashi and Zal sections

In the Ali Bashi and Zal sections, the lithologic units of the Upper Permian successions are subdivided into the Wuchiapingian Julfa Formation, which is dividable into Wuchiapingian Lower and Upper Julfa Beds, and the Changhsingian Ali Bashi Formation, which is subdivided into the Zal Member and the *Paratirolites* Limestone (Fig. 2). The latest Changhsingian Aras Member, or “Boundary Clay”, forms the lowermost beds of the Elika Formation and conformably overlies the *Paratirolites* Limestone. The Elika Formation is subdivided into two parts. The lower part is Early Triassic in age and is composed of thin-bedded limestone and marly limestone with marl and thin-bedded dolomite intercalation. The upper part is Middle Triassic in age and contains medium to thick-bedded dolomites (Glaus, 1964; Seyed-Emami, 2003). This study only addresses the lowermost part of the Elika Formation. The base of the studied sections in both Ali Bashi and Zal sections fall within the uppermost portion of the Wuchiapingian Khachik Formation, which has been assigned to the Wuchiapingian based on the occurrence of the fusulinid foraminiferan *Codonofusiliakkwangsiana* (Ghaderi et al., 2014b). The uppermost part of the Khachik Formation is composed of

dark gray, medium-bedded limestone and is conformably overlain by the Lower Julfa Beds. The Lower Julfa Beds are composed of gray shales interbedded with gray limestones. The Upper Julfa Beds consist of reddish to pinkish limestones with fewer shale intercalations than the Lower Julfa Beds. The Zal Member of the Ali Bashi Formation is predominantly composed of red and purple shales with some limestone intercalations followed by red, nodular, cliff-forming limestones of the *Paratirolites* Limestone. The Aras Member (i.e., boundary clay), which is immediately above the extinction horizon, overlies the *Paratirolites* Limestone and contains mostly red to purplish shales in the Zal section but red and purplish shales interbedded with greenish gray to light gray shales in its upper part in the Ali Bashi section. The platy, thin-bedded limestones with a few light gray to greenish shale interbeds form the basal part of the Elika Formation.

3.2. Lithostratigraphy of the Abadeh sections

The Permian deposits in the Hambast Valley at Abadeh are subdivided into 7 units (units 1–3 of the Surmaq Formation, units 4 and 5 of the Abadeh Formation, and units 6 and 7 of the Hambast Formation) and those of the Lower Triassic are subdivided into 5 units (a–e) (Taraz et al., 1981). In previous studies, the Capitanian-Wuchiapingian (C–W) boundary was placed in the middle part of Unit 5 of the Abadeh Formation (Korte et al., 2004a; Korte and Kozur, 2010). However, based on the recent foraminiferal-based biostratigraphy of the Permian deposits in the Abadeh section, the



(caption on next page)

Fig. 2. Stratigraphic subdivision and lithology of the Upper Permian to lowermost Triassic deposits in Ali Bashi and Zal sections of Julfa. Abbreviations: MIC/MUD = Micrite/mudstone, WACK = wackestone, PACK = packstone, GRAIN = grainstone, Greisba. = Greisbachian, Khach. = Khachik, Parat. L. = *Paratirolites* Limestones, B. C. = “Boundary Clay”, Foram. Bio. = Foraminifer Biozone, Brach. Bio. = Brachiopod Biozone, Cono. Bio. = Conodont Biozone, Ammo. Bio. = Ammonoid Biozone, E. H. = Extinction horizon, P-Tr B. = Permian-Triassic boundary, brachiopod biozones for Ali Bashi section are from Ghaderi et al. (2014b), conodont biozones for Ali Bashi section are from Kozur (2007), Shen and Mei (2010), and Ghaderi et al. (2014a): C. d. = *Clarkinadokouensis*, C. a. = *Clarkina asymmetrica*, C. l. = *Clarkina leveni*, C. g. = *Clarkina guangyuanensis*, C. l. = *Clarkina liyangshanensis*, C. or. = *Clarkina orientalis*, C. s.- C. o. In. = *Clarkina subcarinata*-*Clarkina orientalis* Interval, *Clarkina sub.* = *Clarkina subcarinata*, C. changxingensis = *Clarkina changxingensis*, a = *Clarkina bachmanni*, b = *Clarkina nodosa*, c = *Clarkina yeni*, d = *Clarkina abadehensis*, e = *Clarkina hauschkei*, f = *Hindeodus praeparvus*-*Hindeodus changxingensis*, g = *Merrillina ultima*-*Stepanovites*? mostleri, H. parvus = *Hindeodus parvus*; ammonoid biozones for Ali Bashi section (Ghaderi et al., 2014a; Korn et al., 2016): Vendioicer. U. = *Vendioceras* *Umbonavarum*, I. trans.-Ph. tria. = *Iranites transcaucasius*-*Phisonites triangulus*, D. n. = *Dzhulfites nodosus*, Sh. sh. = *Shevyrevites shevyrevi*, A = *Paratirolites trapezoidalis*, B = *Paratirolites kittli*, C = *Stoyanowites dieneri*, D = *Alibashites mojisovicci*, E = *Abichites abichi*, F = *Abichites stoyanowi*, G = *Arasella minuta*; Conodont biozones for Zal sections (Shen and Mei, 2010; Isaa et al., 2016): C. g. = *Clarkina guangyuanensis*, C. transcauca. = *Clarkina transcaucasica*, = *Clarkina orientalis*, C. o.-C. s. = *Clarkinao rientalis*-*Clarkina subcarinata*, C. sub. = *Clarkina subcarinata*, C. changxingensis = *Clarkina changxingensis*, C. b. = *Clarkina bachmanni*, 1 = *Clarkina nodosa*, 2 = *Clarkina yeni*, 3 = *Clarkina abadehensis*, 3 = *Clarkina hauschkei*, 4 = *Clarkina meishanensis*-*Hindeodus praeparvus*, 5 = *Merrillina ultima*-*Stepanovites*? mostleri; Ammonoid biozones for Zal section in *Paratirolites* Limestones are the same as Ali Bashi section. The one foraminiferal biozone for both Ali Bashi and Zal sections is from Ghaderi et al. (2014b, 2016): C. kwang. = *Codonofusiellakwangsiiana*. Samples labelled as J1-2 to J118 were collected from both limestones and shales of the Ali Bashi section and samples labelled as JL were collected from limestones interbeds of the Zal Member in this section. Samples labelled Z belongs to Khachik through Upper Julfa Bed in Zal section, those labelled as ZS for Zal Member of the Zal section, those labelled as ZP for *Paratirolites* Limestones of the Zal section and those labelled as ZT for Elika Formation in Zal section.

C-W boundary is now placed within the lower part of Subunit 4b of Unit 4 of the Abadeh Formation, which contains the first appearances of *Pseudodunbarula* sp. and *Codonofusiellakwangsiiana* (Shahinfar et al., 2020; Arefifard and Payne, 2020). Therefore, the Upper Permian strata include Wuchiapingian middle and upper parts of Subunit 4b of Unit 4 and Wuchiapingian Unit 5 of the Abadeh Formation, Wuchiapingian Unit 6, and Changhsingian Unit 7 of the Hambast Formation and the uppermost Changhsingian boundary clay (Shahinfar et al., 2020; Arefifard et al., 2022). The Elika Formation conformably overlies the Upper Permian deposits in the Abadeh section; it starts with the uppermost Changhsingian boundary clay and continues with Lower Triassic limestones (Fig. 3). The middle and upper parts of Subunit 4b of the Abadeh Formation, which only crop out in the Abadeh-1 section, contain gray shales and gray to dark gray shaly limestone and gray limestone. Unit 5 of the Abadeh Formation consists mainly of gray to dark gray limestone with few gray shales, especially in its lower part. Unit 6 of the Hambast Formation includes alternations of light green shales and light gray, thin-bedded, micritic limestone. Unit 7 of the Hambast Formation is composed of red thin- to medium-bedded limestone exhibiting mostly nodular or finely wavy bedding. The uppermost Changhsingian boundary clay contains greenish and dark gray shales with few intercalations of light gray, thin-bedded limestones. The base of Unit “a” of the Elika Formation are limestones with structures interpreted and described alternatively as “thrombolite” (Taraz et al., 1981; Baghbani, 1993; Heydari et al., 2000), a “shallow water syn-sedimentary cement layer” (Heydari et al., 2003), “calcite fan” (Leda et al., 2014), and “sponge microbial bioherms” (Friesenbichler et al., 2018; Baud et al., 2021). These microbial limestones are followed by platy limestones of the *Claraia* Beds.

There are some differences in lithology and thickness of the Wuchiapingian Subunit 4b and Unit 5 of the Abadeh Formation between the Abadeh-1 and Abadeh-2 sections despite being only 2 km apart. The Abadeh-1 section is on the southeast flank of the main Hambast Valley (N 30°54'01.5", E 53°12'34.3"), about 35 km southeast of the town of Abarkuh. The Abadeh-2 section is on the NE side of the main Hambast Valley (N 30°55'04.8", E 53°12'14.5"), about 200 m beyond the entrance of the Hambast Valley and approximately 2 km northwest of the first section. Although the Abadeh Formation is exposed in the Abadeh-2 section, most of its thickness belongs to the upper Capitanian Subunit 4a and only 1 m of Unit 5 is exposed in this section. In fact, the cliff-forming gray to dark gray limestones of Unit 5 in the Abadeh-1 section correlate to Subunit 4a of the Abadeh-2 section based on their foraminiferal contents (Shahinfar et al., 2020; Arefifard and Payne, 2020). Therefore, the biostratigraphy of the Abadeh-2 section conflicts with this lithostratigraphic correlation; the foraminifera of the upper part of the Abadeh Formation at the Abadeh-2 section occur in Subunit 4b in the Abadeh-1 section, suggesting that the upper limestones

belonging to Unit 5 of the Abadeh Formation are time transgressive. These differences between the two sections indicate lateral facies variation that might reflect a paleoenvironmental gradient or, possibly, an active syndepositional fault between the two sites.

4. Materials and methods

4.1. Thin section study

A total of 324 samples of latest Capitanian to Early Triassic age were collected: 101 samples from the Ali Bashi section, 40 samples from the Zal section, 121 samples from the Abadeh-1 section and 63 samples from the Abadeh-2 section. We measured $\delta^{13}\text{C}_{\text{carb}}$, $\delta^{18}\text{O}_{\text{carb}}$ and $\delta^{13}\text{C}_{\text{org}}$ for Ali Bashi and Zal sections but only $\delta^{13}\text{C}_{\text{carb}}$ and $\delta^{18}\text{O}_{\text{carb}}$ for Abadeh sections 1 and 2 and $\delta^{13}\text{C}_{\text{org}}$ results from uppermost Permian to lowermost Triassic deposits from a section studied by Korte et al. (2004a), here referred to as Abadeh Section 3. Polished thin sections were prepared from limestone beds of these four sections for petrographic examination and to evaluate the preservation of isotopic compositions.

4.2. $\delta^{18}\text{O}$ and $\delta^{13}\text{C}$ of bulk carbonate

For isotope analysis, powder was drilled from fresh surfaces of hand samples, focusing on homogeneous bulk-rock material. Veins and weathered portions were avoided. Aliquots between 300 and 700 μg of bulk rock carbonate powders were transferred into glass vials and reacted at 70 °C with ~50 μL manually added anhydrous phosphoric acid after sealing and removing atmospheric gases with He. Obtained CO_2 was analyzed for carbon and oxygen isotope ratios by using the IsoPrime triple collector Isotope Ratio Mass Spectrometer at the IGN of the University of Copenhagen. Sample-weight-dependent isotope fractionation was corrected by applying the calibration curves constructed after multiple measurements of the in-house standard LEO (Carrara Marble; $\delta^{13}\text{C} = +1.96\ \text{\textperthousand}$ V-PDB; $\delta^{18}\text{O} = -1.93\ \text{\textperthousand}$ V-PDB) covering the entire sample weight range (see also Ullmann et al., 2013). The analytical precision (2sd) calculated from repeated measurements of LEO was better than 0.1 ‰ for $\delta^{13}\text{C}$ and better than 0.2 ‰ for $\delta^{18}\text{O}$.

4.3. $\delta^{13}\text{C}$ of bulk organic matter

85 shaly samples of latest Capitanian to Early Triassic age were analyzed, comprising 46 samples from the Ali Bashi section and 39 samples from the Zal section. Drilled bulk-rock powders were decarbonated using 6 M hydrochloride acid. The acid remains were removed afterwards by multiple rinsing, centrifugation and discarding supernatant fluids. The remaining non-carbonate fraction was freeze dried. Organic carbon isotope ratios ($\delta^{13}\text{C}_{\text{org}}$) were determined by using the

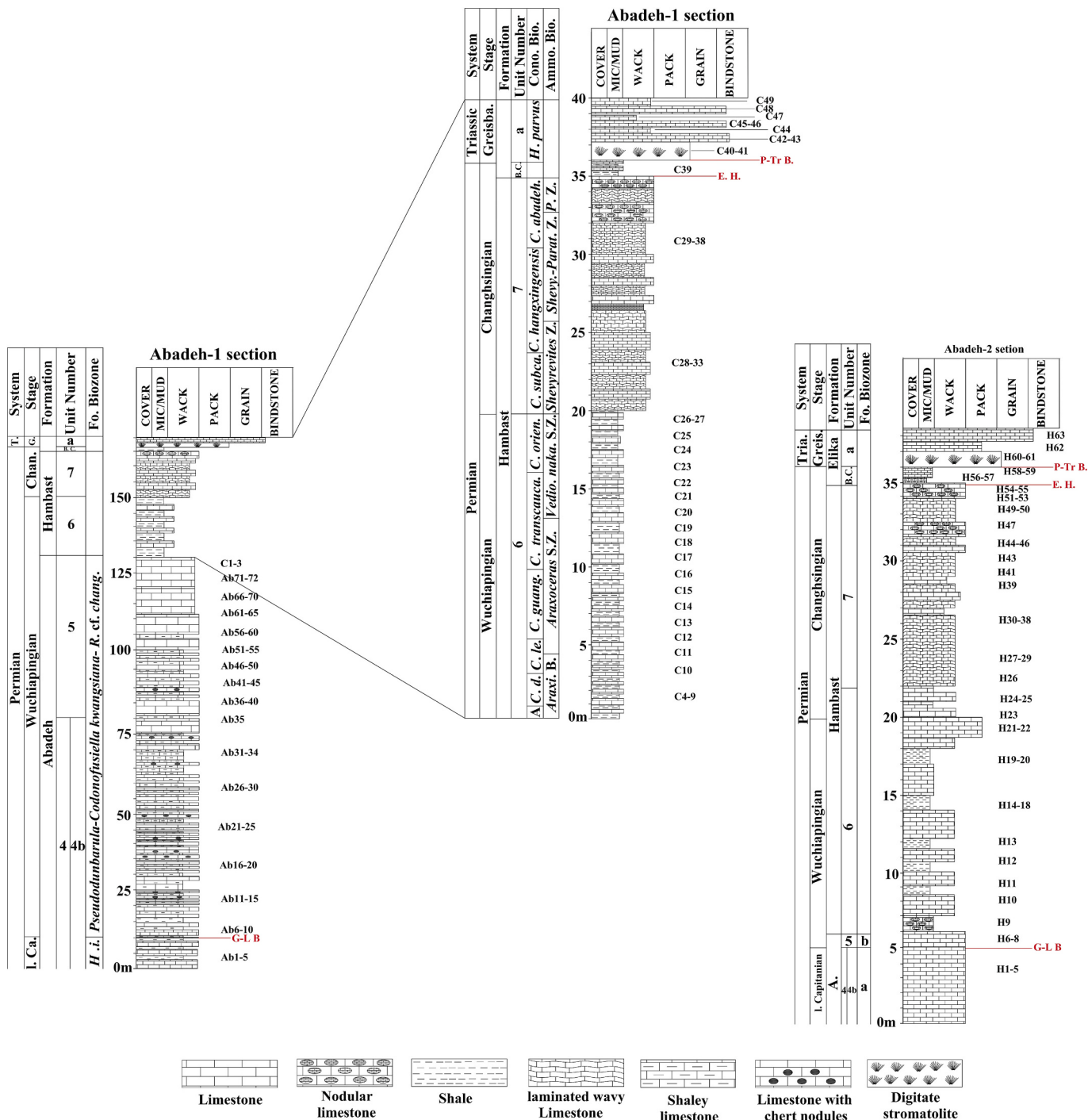


Fig. 3. Lithology and stratigraphic subdivision of the Upper Permian to lowermost Triassic sediments in the Abadeh-1 and Abadeh-2 sections of the Hambast Valley. Abbreviations: A. = Abadeh, Am. and Br. B. = Ammonoid and brachiopod Biozones, Fo. Biozone = Foraminifer Biozone, E. = Elika, Chan. = Changhsingian, G. = Giresbachian, Gries. = Griesbachian, T. = Triassic, Tria. = Triassic, B. C. = “Boundary Clay”, Z. = Zone, S.Z. = Subzones, E. H. = Extinction horizon, G-L B. = Guadalupian-Lopingian boundary, P-Tr B. = Permian-Triassic boundary, Conodont biozones (Kozur, 2007; Shen and Mei, 2010): A = *Clarkina? postbitteri*, C. d. = *Clarkina dokouensis*, C. le. = *Clarkina leveni*, C. guang. = *Clarkina guangyuanensis*, C. transcaucasica = *Clarkina transcaucasica*, C. orie. = *Clarkina orientalis*, C. subca. = *Clarkina subcarinata*, C. changxingensis = *Clarkina changxingensis*, C. Abadeh. = *Clarkina abadehensis*, H. parvus = *Hindeodus parvus*. Ammonoid and brachiopod biozones (Taraz et al., 1981): Araxi. Beds = Araxilevis Beds, Vedio. naka. = *Vedioceras nakamurai*, Shevy.-Para. = *Shevyrevires-Paratirolites*, P. = *Paratirolites*. Foraminifer biozones (Shahinfar et al., 2020): a = *H. irreg.* = *Hemigordius irregulariformis*, b = R. cf. chang. = *Reichelina cf. changhsingensis*. Samples labelled as Ab1 in Abadeh section are collected from lower part of the subunit 4b and most part of the Unit 5 of the Abadeh Formation and those labelled as C are from uppermost part of the Unit 5 of the Abadeh Formation. Samples labelled as H are from upper part of the Unit 4 to lowermost part of the Elika Formation in Abadeh-2 section.

Euro EA Elemental Analyzer coupled with the Iso Prime Gas Source Isotope Ratio Mass Spectrometer at the Department of Geosciences and Natural Resource Management, University of Copenhagen. The carbon isotope ratios were normalized to the PDB scale using the in-house AKskill-9 standard ($\delta^{13}\text{C}$: -25.30 ‰). The reproducibility of the $\delta^{13}\text{C}_{\text{org}}$ values was better than 0.1 ‰.

5. Results

5.1. Bulk carbonate $\delta^{13}\text{C}_{\text{carb}}$ and $\delta^{18}\text{O}_{\text{carb}}$, bulk rock $\delta^{13}\text{C}_{\text{org}}$ and $\Delta^{13}\text{C}$

5.1.1. Ali Bashi and Zal sections

The Upper Permian to lowermost Triassic $\delta^{13}\text{C}_{\text{carb}}$ values range widely, from -2.7 ‰ to 4.8 ‰ ($n = 101$, mean = 3 ‰, σ (standard deviation) = 1.8) in the Ali Bashi section, and from -0.5 ‰ to 4.2 ‰ ($n = 40$, mean = 2.8 ‰, $\sigma = 1.4$) in the Zal section (Figs. 4–5, Data Files S1–S2). The carbonate $\delta^{13}\text{C}$ values throughout the Wuchiapingian uppermost part of the Khachik Formation and Julfa Beds in both the Ali Bashi and Zal sections range between 3 ‰ and 4 ‰ (for the Ali Bashi section: $n = 69$, mean = 3.7 ‰, $\sigma = 0.6$ and for the Zal section: $n = 23$, mean = 3.6, $\sigma = 0.3$), but in the uppermost portion of the Julfa Beds in the Ali Bashi section the differences between consecutive samples are as large as 2 ‰. The overall magnitude of $\delta^{13}\text{C}_{\text{carb}}$ fluctuations in the Wuchiapingian part of the studied sections is around 1 ‰ or less. No significant shift is recognizable between the Wuchiapingian Julfa Beds and the Changhsingian Zal Member in either the Ali Bashi or the Zal section.

The Changhsingian Zal Member of the Ali Bashi and Zal sections generally contains $\delta^{13}\text{C}_{\text{carb}}$ values of 3 ‰. In the upper part of the Zal Member in the Ali Bashi section, one sample has a $\delta^{13}\text{C}_{\text{carb}}$ closer to 1.5 ‰, which we interpret to be an outlier because it is not part of any longer-term trend. These values are followed by an abrupt return to 3 ‰ for the rest of the Zal Member. The $\delta^{13}\text{C}_{\text{carb}}$ values in the upper Changhsingian *Paratirolites* Limestone of the Ali Bashi and Zal sections are near 2 ‰, about 1 ‰ lighter than those in the Zal Member. There is a sharp decrease of 1.6 ‰ in the topmost part of the upper Changhsingian *Paratirolites* Limestone of the Ali Bashi section, whereas in the Zal section the corresponding decline is only ~0.3 ‰. This negative shift in $\delta^{13}\text{C}_{\text{carb}}$ continues in the uppermost Changhsingian Aras Member, reaching almost 2 ‰ in the Ali Bashi section and 1.5 ‰ in the Zal section, which is comparable to the values measured in the lowermost beds of the Lower Triassic limestones of the Erika Formation in both sections.

The Oxygen isotope values vary significantly through the Upper Permian, ranging between -7.3 ‰ and -2.8 ‰ ($n = 101$, mean = -5 ‰, $\sigma = 1.1$) in the Ali Bashi section and between -7.2 ‰ and -2.5 ‰ ($n = 40$, mean = -5.2 ‰, $\sigma = 1.1$) in the Zal section (Figs. 4–7, Data Files S1–S3). The $\delta^{13}\text{C}_{\text{org}}$ values vary widely in the Upper Permian and lowermost Triassic deposits. They range between -27.8 ‰ and -20.5 ‰ in the Ali Bashi section ($n = 46$, mean = -25.5, $\sigma = 1.5$) and between -28.3 ‰ and -20.8 ‰ in the Zal section ($n = 35$, mean = -25.4, $\sigma = 1.4$) (Figs. 4–5; Data Files S1–S2). For the uppermost part of the Khachik Formation, which is Wuchiapingian in age, the differences in $\delta^{13}\text{C}_{\text{org}}$ between stratigraphically adjacent samples are small (about 1 ‰ to 2

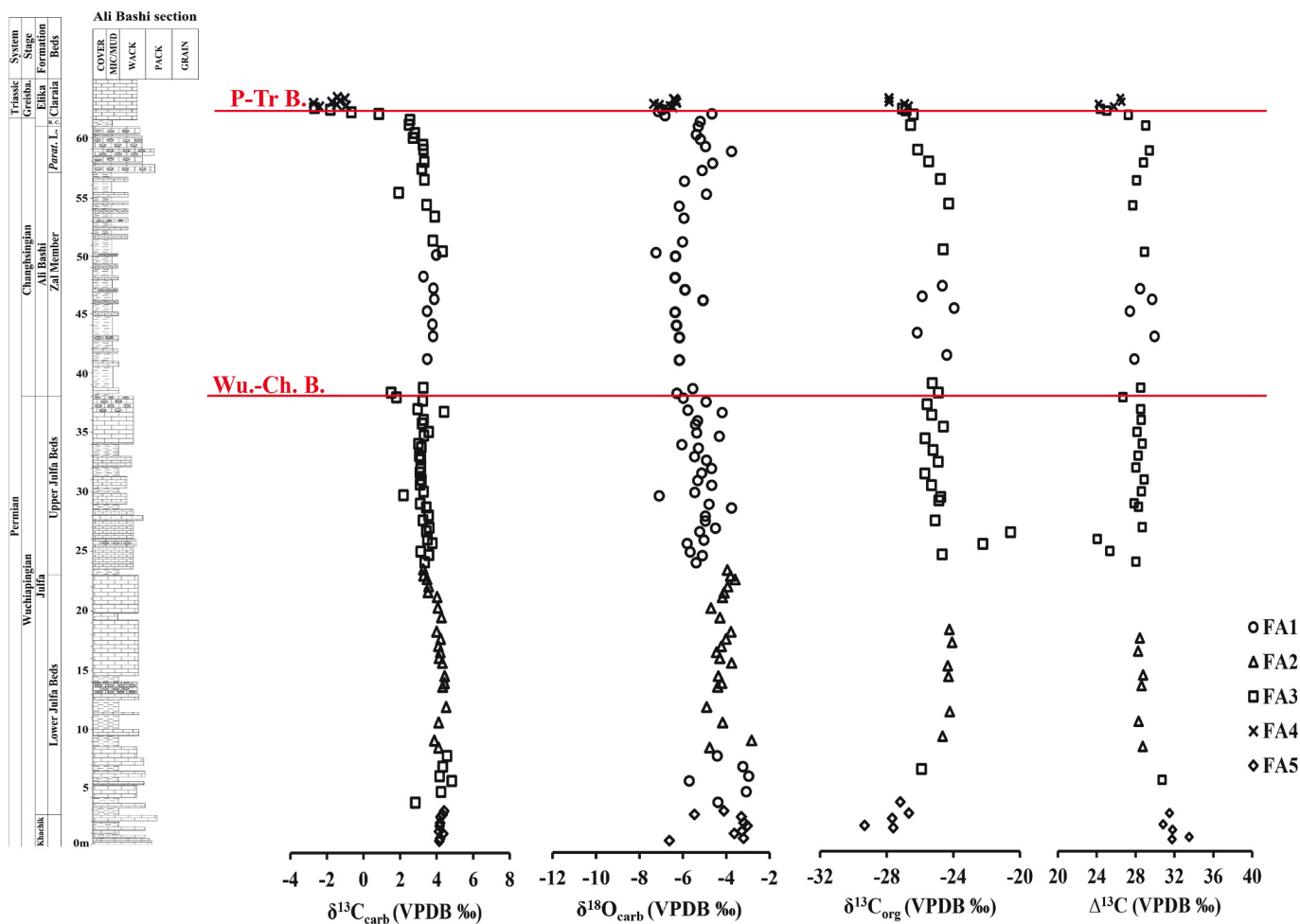


Fig. 4. $\delta^{13}\text{C}_{\text{carb}}$, $\delta^{13}\text{C}_{\text{org}}$, $\Delta^{13}\text{C}$ and $\delta^{18}\text{O}_{\text{carb}}$ data plotted against the stratigraphy and lithology of Ali Bashi section. Abbreviations: Wu.-Ch. B. = Wuchiapingian–Changhsingian boundary, P-Tr B. = Permian-Triassic boundary, FA1 = Lime mudstone, FA2 = Lime mudstone-bioclastic wackestone, FA3 = bioclastic wackestone, FA4 = Recrystallized bioclastic wackestone, FA5 = Recrystallized bioclastic packstone, for more abbreviations see the caption of Fig. 2.

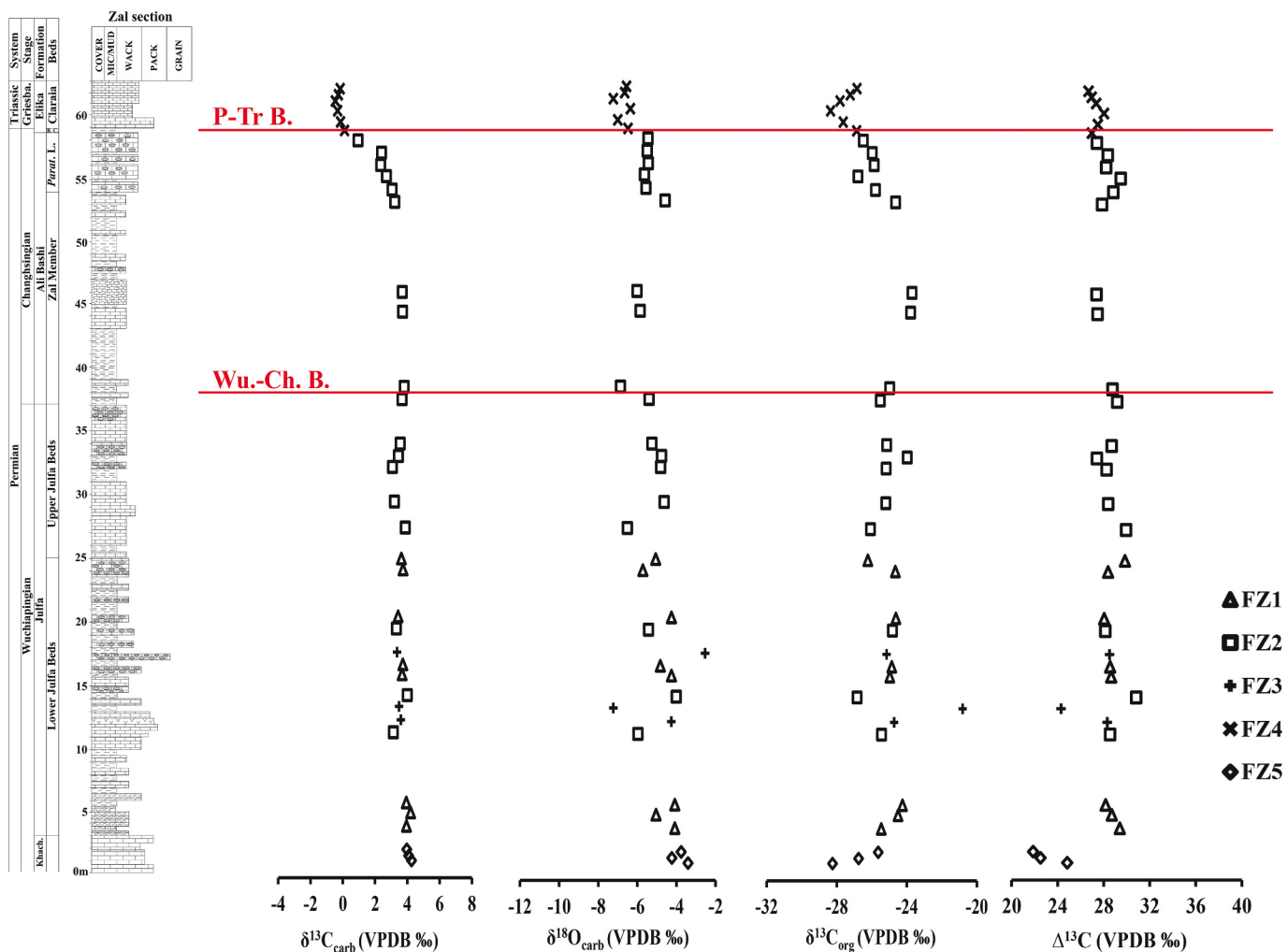


Fig. 5. $\delta^{13}\text{C}_{\text{carb}}$, $\delta^{13}\text{C}_{\text{org}}$, $\Delta^{13}\text{C}$ and $\delta^{18}\text{O}_{\text{carb}}$ data plotted against lithology and stratigraphy of the Zal section. Abbreviations: Wu.-Ch. B. = Wuchiapingian-Changhsingian boundary, FZ1 = Lime mudstone-bioclastic wackestone, FZ2 = Bioclastic wackestone, FZ3 = Bioclastic packstone, FZ4 = Recrystallized bioclastic packstone, FZ5 = Recrystallized bioclastic wackestone, for more abbreviations see the caption of Fig. 2.

(‰). The $\delta^{13}\text{C}_{\text{org}}$ compositions in the uppermost part of the Khachik Formation vary between -29.3 ‰ and -26.7 ‰ in the Ali Bashi section and from -28.2 ‰ to -25.6 ‰ in the Zal section. Starting from Lower Julfa Beds, there is an increase in $\delta^{13}\text{C}_{\text{org}}$ of $\sim 2\text{ ‰}$ in the Ali Bashi section and $\sim 1\text{ ‰}$ in the Zal section. The mean $\delta^{13}\text{C}_{\text{org}}$ values are near -25 ‰ in the Wuchiapingian and lower Changhsingian in both sections, the $\delta^{13}\text{C}_{\text{org}}$ values does not demonstrate any remarkable change across the Wuchiapingian-Changhsingian (W-Ch) boundary. The mean $\delta^{13}\text{C}_{\text{org}}$ values decline by approximately 1.5 ‰ in the upper Changhsingian, indicative of the P-Tr boundary. In the lowermost Triassic Elika Formation, the mean of $\delta^{13}\text{C}_{\text{org}}$ remains near -27 ‰ in both sections, which is the same as uppermost part of the Changhsingian.

The $\Delta^{13}\text{C}$ values range from 24 ‰ to 33.5 ‰ ($n = 46$, mean = 28.3 ‰ , $\sigma = 1.9$) in the Upper Permian to lowermost Triassic strata in the Ali Bashi section and from 24.3 ‰ to 30.8 ‰ ($n = 35$, mean = 28.1 ‰ , $\sigma = 1.12$) in the Zal section (Figs. 4–5, Data Files S1–S2). The average $\Delta^{13}\text{C}$ values are similar for the Wuchiapingian and Changhsingian samples ($\sim 28\text{ ‰}$) with a slight decrease in the Changhsingian samples. A negative shift occurs in the uppermost Changhsingian, with a magnitude of about 2 ‰ in the Ali Bashi section and about 1 ‰ in the Zal section. This negative trend continues into the lowermost Triassic Elika Formation.

5.1.2. Abadeh sections

The $\delta^{13}\text{C}_{\text{carb}}$ values show a wide range in Upper Permian to

lowermost Triassic deposits, from 5.6 ‰ to -0.4 ‰ ($n = 121$, mean = 3.2 ‰ , $\sigma = 1.2$) in the Abadeh-1 section (Fig. 6, Data File S3) and from 4.9 ‰ to -0.3 ‰ ($n = 63$, mean = 3.5 ‰ , $\sigma = 1.2$) in the Abadeh-2 section (Figs. 7, Data File S3). There is a near-constant value of 4 ‰ for the Capitanian part of the Abadeh-2 section and about 3 ‰ for the Abadeh-1 section. The Capitanian-Wuchiapingian transition does not exhibit a negative excursion in either section. The Wuchiapingian samples of the middle and upper portions of Subunit 4b and Unit 5 of the Abadeh Formation in the Abadeh-1 section have $\delta^{13}\text{C}_{\text{carb}}$ values between 3 and 4 ‰ . Starting from Unit 6 of the Hambast Formation (Wuchiapingian), there is a negative excursion of $\sim 1.6\text{ ‰}$ in $\delta^{13}\text{C}_{\text{carb}}$ in the Abadeh-1 section (Fig. 6) but not in the Abadeh-2 section (Fig. 7). The Changhsingian C-isotope profiles from the Abadeh-1 and Abadeh-2 sections are generally comparable with the Ali Bashi and Zal sections. A near-constant value of 3 ‰ occurs throughout Unit 7 of the Hambast Formation (Changhsingian) in the Abadeh-1 section. In the Abadeh-2 section, by contrast, the Changhsingian $\delta^{13}\text{C}_{\text{carb}}$ values are more variable, mostly ranging between 3.5 ‰ and 4.2 ‰ but including occasional values as light as 2.4 ‰ in the middle part of Unit 7. An abrupt negative shift in $\delta^{13}\text{C}_{\text{carb}}$ of about 3.2 ‰ and 3.6 ‰ in the uppermost portion of Unit 7 in the Abadeh-1 and Abadeh-2 sections, respectively, occurs and continues into the uppermost Changhsingian boundary clay and lowermost Triassic deposits.

$\delta^{18}\text{O}_{\text{carb}}$ from uppermost Guadalupian to lowermost Triassic samples

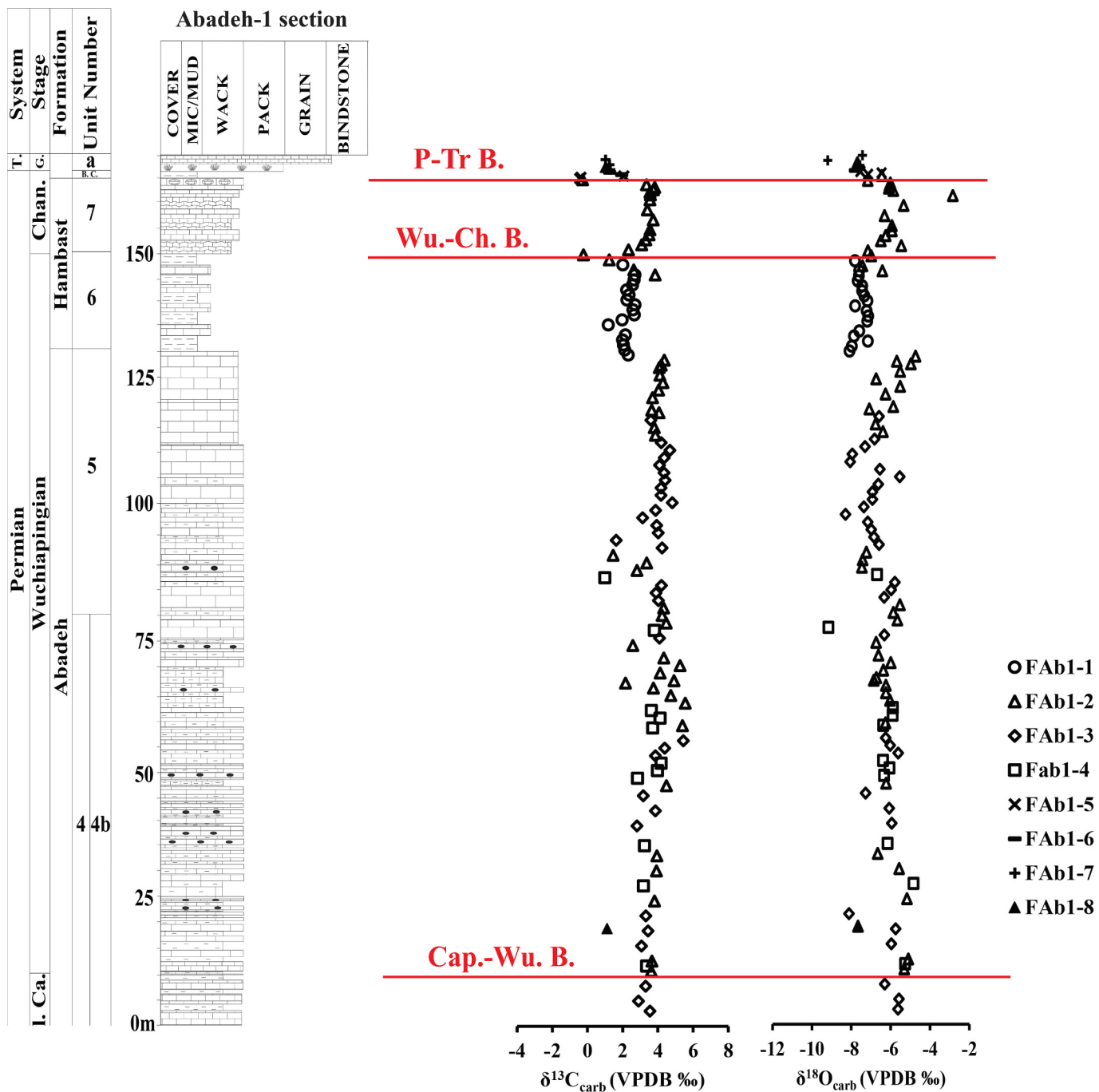


Fig. 6. $\delta^{13}\text{C}_{\text{carb}}$ and $\delta^{18}\text{O}_{\text{carb}}$ data plotted against the stratigraphy of the Abadeh-1 section, Julfa region, SW Iran. Abbreviations: Cap.-Wu. B. = Capitanian-Wuchiapingian boundary, Wu.-Ch. B. = Wuchiapingian-Changhsingian boundary, FAb1-1 = Mudstone, FAb1-2 = Bioclastic wackestone partly recrystallized, FAb1-3 = Bioclastic algal packstone partly recrystallized, FAb1-4 = Dolosparite, FAb1-5 = Sponge microbial buildups, FAb1-6 = Laminated peloidal bindstone, FAb1-7 = Microbial with sparry calcite spheres, FAb1-8 = Laminated lime bindstone, for more abbreviations see the caption of Fig. 3.

ranges between -9.2 ‰ and -2.8 ‰ ($n = 121$, mean = -6.6 ‰ , $\sigma = 0.94$) in the Abadeh-1 section and between -11.1 ‰ and -3.2 ‰ ($n = 63$, mean = -7.6 ‰ , $\sigma = 1.74$) in the Abadeh-2 section (Data File S3). We compared the $\delta^{13}\text{C}_{\text{carb}}$ data measured in Abadeh sections 1 and 2 as part of this study with $\delta^{13}\text{C}_{\text{org}}$ data previously reported by Korte et al. (2004a) for the Abadeh-3 section. The $\delta^{13}\text{C}_{\text{org}}$ trend of the Abadeh-3 section is based on a few samples from the Wuchiapingian Units 5 and 6, and more samples from Unit 7 of the Hambast Formation and Unit a of the Lower Triassic Elikfa Formation (Korte et al., 2004a) (Fig. 8, Data File S3). The $\delta^{13}\text{C}_{\text{org}}$ values range widely, from -28.5 ‰ to -23.6 ‰ ($n = 22$, mean = -26 ‰ , $\sigma = 1.3$), in the Upper Permian to Lower Triassic strata.

The average value of $\delta^{13}\text{C}_{\text{org}}$ for whole Upper Permian is $\sim -25\text{ ‰}$ at Abadeh, which is the same for the Wuchiapingian and Changhsingian. There is a recognizable decline of $\sim -2\text{ ‰}$ for $\delta^{13}\text{C}_{\text{org}}$ starting from the basal of the Lower Triassic Unit a. The average value of the $\delta^{13}\text{C}_{\text{org}}$ for the Lower Triassic samples is about -26 ‰ , which is about 1 ‰ lower than that of the Upper Permian samples. The Lower Triassic $\delta^{13}\text{C}_{\text{org}}$ values vary between 1 ‰ to 2 ‰ .

The $\Delta^{13}\text{C}$ values range from 24.8 ‰ to 31.3 ‰ ($n = 22$, mean = 28 ‰ , $\sigma = 1.8$) in the Abadeh section (Korte et al., 2004a) (Fig. 8, Data File S3). Similarly to the Ali Bashi section, a negative shift in $\delta^{13}\text{C}_{\text{carb}}$ starts before the negative excursion in $\delta^{13}\text{C}_{\text{org}}$, creating a decrease in $\Delta^{13}\text{C}$ of ca. 2 ‰ .

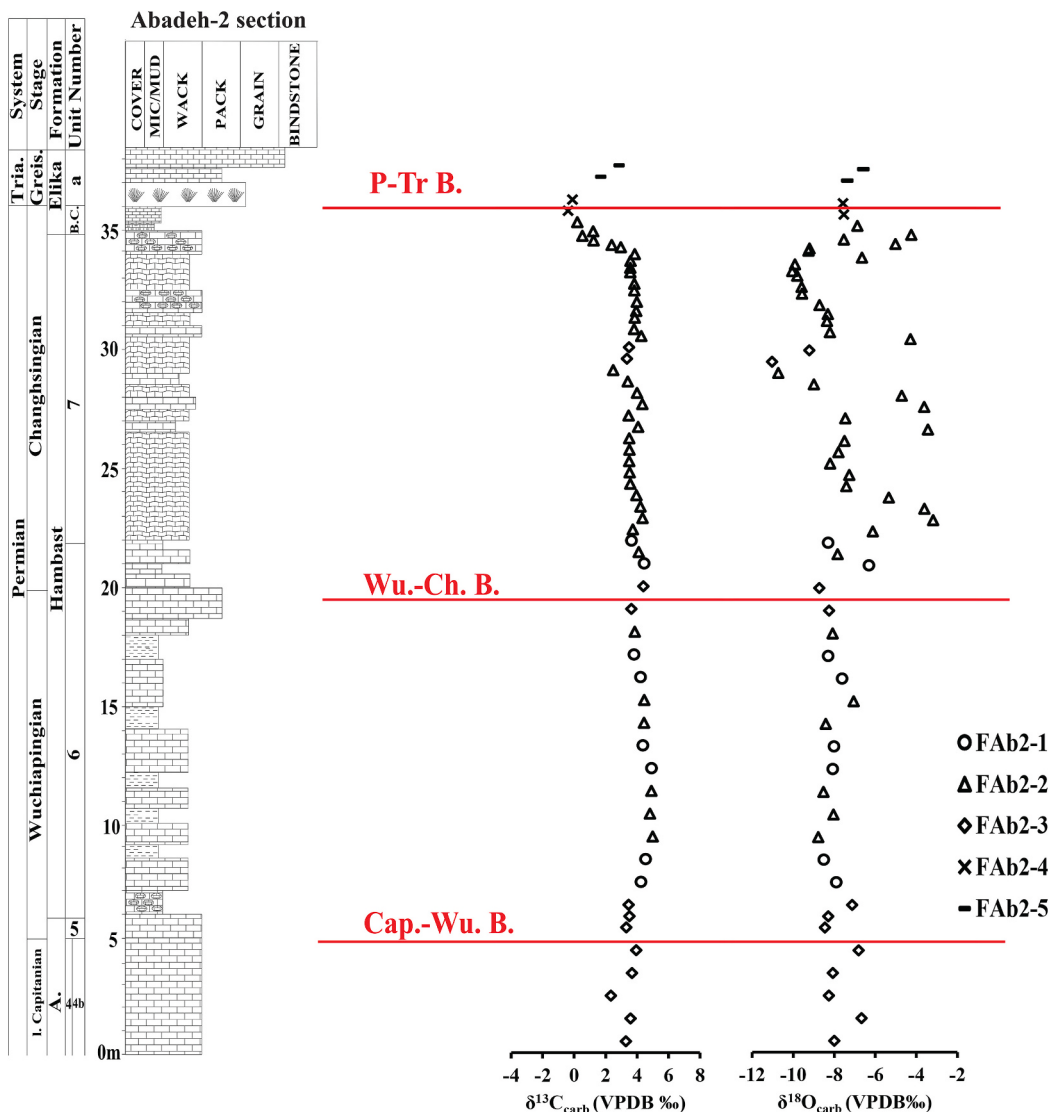


Fig. 7. $\delta^{13}\text{C}_{\text{carb}}$ and $\delta^{18}\text{O}_{\text{carb}}$ data plotted against the stratigraphy of the Abadeh-2 section, Abadeh region, SW Iran. Abbreviations: Cap-Wu B. = Capitanian-Wuchiapingian boundary, Wu.-Ch. B. = Wuchiapingian-Changhsingian boundary, FAb2-1 = Mudstone, FAb2-2 = Bioclastic wackestone, FAb2-3 = Bioclastic intraclastic packstone, FAb2-4 = Sponge microbial buildups, FAb2-5 = Laminated peloidal bindstone, for more abbreviations see the caption of Figs. 3 and 6. The red lines indicating stage boundaries in this figure are aligned with those in Fig. 3.

in the uppermost portion of Unit 7 of the Hambast Formation. This decreasing trend continues to the extinction interval. The microbial buildups at the base of the Elika Formation show a positive shift of $\Delta^{13}\text{C}$ of about 2.5 ‰, which is followed by a decrease in the upper beds.

6. Discussion

6.1. Preservation versus alteration of the geochemical signals

6.1.1. Petrographic studies

To evaluate the preservation of isotopic compositions in the studied bulk carbonates, thin sections of most of the limestone samples have been petrographically examined (Figs. 9–11). Most of the Upper Permian samples deposited in open-marine, mid- to outer-ramp settings (Leda et al., 2014; Arefifard and Baud, 2022) are wackestone or packstone, containing micritic matrix with varying proportions of allochems, especially skeletal grains, in which calcite cement has filled the intra-particle pores or the whole skeletal grains are filled with calcite. The micritic matrix shows small voids filled with calcite cements. There is no indication of early marine cement types, such as isopachous rims of

fibrous or radial fibrous cement. Recrystallization occurred sporadically in the micritic matrix (Figs. 9–11). In shallow-water deposits of the lowermost beds of the Lower Triassic Elika Formation, the microfacies-related recrystallization is even more pronounced than that of the Upper Permian deposits. This difference is evidenced by sparry calcite spheres in bioclastic wackestone where most of the micrite was replaced by calcite crystals with minor remains of primary micrite (Fig. 10).

6.1.2. Facies-related isotope trends

The $\delta^{18}\text{O}_{\text{carb}}$ versus $\delta^{13}\text{C}_{\text{carb}}$ plots of Ali Bashi ($p\text{-value} = 2.7 * 10^{-5}$, $r^2 = 0.19$), Zal ($p\text{-value} = 0.56$, $r^2 = 0.01$), Abadeh-1 ($p\text{-value} = 2.5 * 10^{-4}$, $r^2 = 0.12$), and Abadeh-2 ($p\text{-value} = 0.21$, $r^2 = 0.03$) show limited correlation between carbon and oxygen isotope ratios. The correlations are statistically significant for Ali Bashi and Abadeh-1, but even in these sections the predictive value is relatively weak. Three different deep-water facies types in mid- to outer-shelf settings occur in the Ali Bashi section, including lime mudstone (FA1), lime mudstone-bioclastic wackestone (FA2) and bioclastic wackestone (FA3). The $\delta^{18}\text{O}_{\text{carb}}$ versus $\delta^{13}\text{C}_{\text{carb}}$ scatter plots of these samples show potentially different facies-related trends in the Upper Permian deposits (Fig. 12a,b, Data

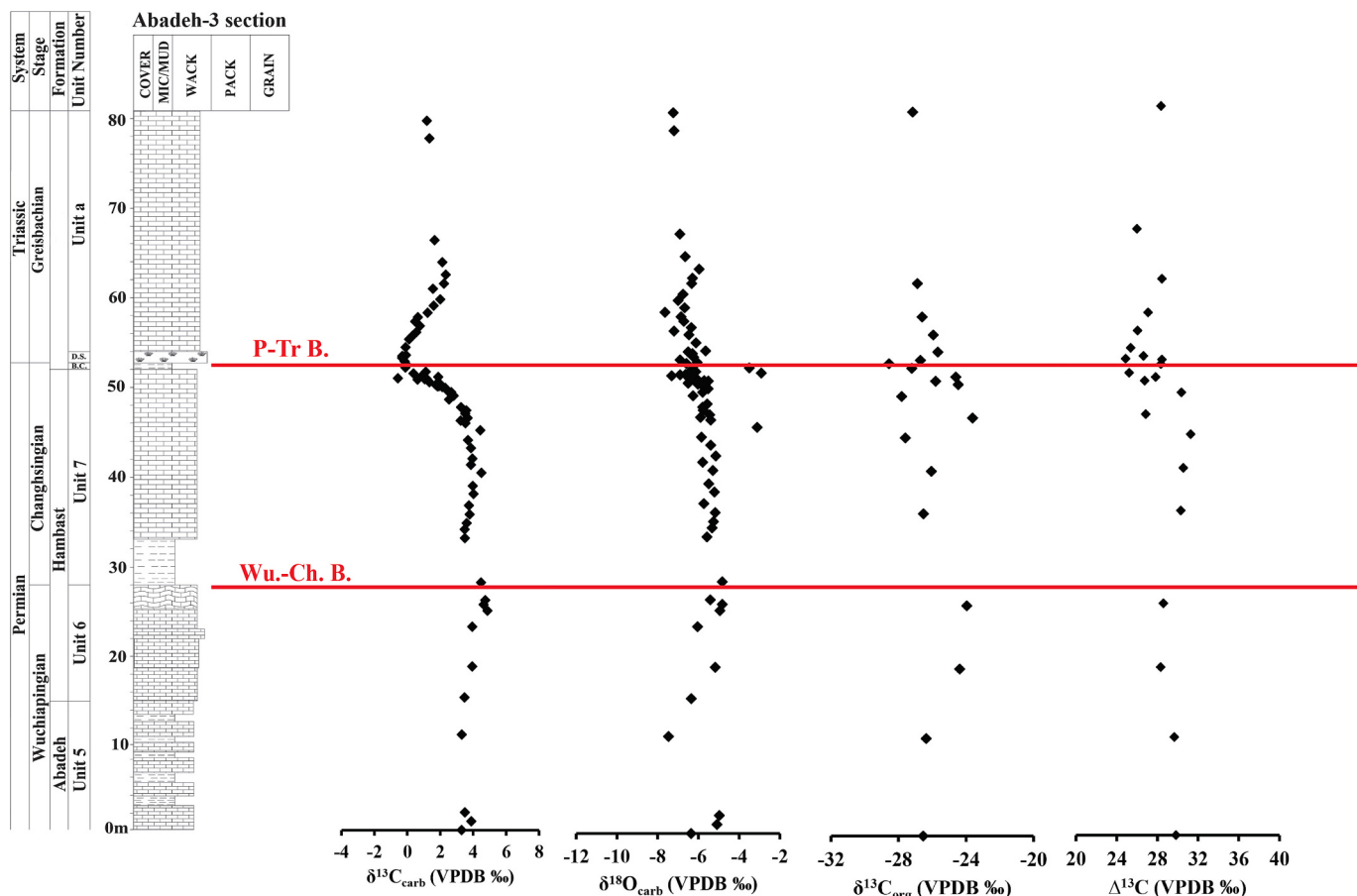


Fig. 8. $\delta^{13}\text{C}_{\text{carb}}$, $\delta^{13}\text{C}_{\text{org}}$, $\Delta^{13}\text{C}$ and $\delta^{18}\text{O}_{\text{carb}}$ data plotted against the stratigraphy of the Abadeh-3 section, Hambast Valley, NW Iran (data replotted from Korte et al., 2004a). Abbreviations: B. C. = “Boundary Clay”, D. S. = Digitate stromatolite, P-Tr B. = Permian-Triassic boundary, Wu.-Ch. B. = Wuchiapingian-Changhsingian boundary.

Files S1 and S4). Akaike Information Criterion (AIC)-based model comparison indicates that a model allowing for different slopes and intercepts by facies outperforms a model of $\delta^{13}\text{C}_{\text{carb}}$ simply as a function of $\delta^{18}\text{O}_{\text{carb}}$ ($\delta^{13}\text{C} \sim \delta^{18}\text{O}$, AIC: 256.07; $\delta^{13}\text{C} \sim \delta^{18}\text{O}^*$ facies, AIC: 249.46); however, none of the slopes returned in the more complex model are statistically significant and none of the facies differ significantly in their calculated intercepts, indicating that this more complex model adds little, if any, predictive value (Fig. S5).

Petrographic observations show that some skeletal grains and micrite in Upper Permian and lowermost Triassic samples from both the Julfa and Abadeh sections were recrystallized to microspar and sparite, suggestive of a primary aragonite mineralogy (Figs. 9–10). The Sr content of the Upper Permian strata in the Hambast Valley (i.e., for the Abadeh section) is high, in the range of 1500–5500 ppm (Heydari et al., 2000), which is consistent with sediment originally dominated by aragonite. However, the Sr concentration is moderate in lowermost Triassic samples from Abadeh, 600–950 ppm (Heydari et al., 2000), suggesting diagenetic Sr loss or originally mixed aragonite and calcite mineralogies. The trend of correlation between $\delta^{13}\text{C}_{\text{carb}}$ and $\delta^{18}\text{O}_{\text{carb}}$ of Upper Permian deep-water deposits in the Zal section is similar across facies (1, 2 and 4), suggesting alteration by similar diagenetic fluids and processes (Figs. 12c,d; Data Files S2 and S4). AIC-based model comparison indicates that a model of $\delta^{13}\text{C}_{\text{carb}}$ simply as a function of $\delta^{18}\text{O}_{\text{carb}}$ outperforms a model that includes an interaction with facies type ($\delta^{13}\text{C} \sim \delta^{18}\text{C}$ AIC: 63.09; $\delta^{13}\text{C} \sim \delta^{18}\text{O}^*$ facies AIC: 65.46; Fig. S5). The resemblance of the trends in the Zal section suggests shared primary and diagenetic end members among facies associations, with differences among facies due

to the extent of diagenetic alteration of the primary composition. The correlation lines between $\delta^{13}\text{C}_{\text{carb}}$ and $\delta^{18}\text{O}_{\text{carb}}$ for three examined facies of the Upper Permian deposits in the Abadeh-2 section are nearly indistinguishable, suggesting shared primary and diagenetic end members among facies associations (Fig. 12).

6.1.3. Preservation of the carbon isotope records in study sections

Diagenetic processes can alter the carbon isotope compositions of marine carbonates and this would complicate the interpretation of the primary carbon-isotope trends; however, several lines of evidence indicate that the $\delta^{13}\text{C}_{\text{carb}}$ values from the sections in Iran largely record primary variations. First, there is no significant correlation between the $\delta^{18}\text{O}_{\text{carb}}$ and $\delta^{13}\text{C}_{\text{carb}}$ in any of the studied sections (Fig. 12). Second, all samples from the Ali Bashi and Zal sections and more than 97 % of the samples from the Abadeh-1 section have $\delta^{18}\text{O}$ greater than -8 ‰ (Figs. 4–6), arguing against substantial meteoric alteration or alteration at high temperature during deep burial (Derry et al., 1992; Kaufman et al., 1993; Kaufman and Knoll, 1995). In contrast to other sections, in the Abadeh-2 section, $\delta^{18}\text{O}_{\text{carb}}$ values of 27 samples (53 % of the samples) are lighter than -8 ‰ , indicative of alteration by meteoric fluids or during deep burial at high temperature. However, the $\delta^{13}\text{C}_{\text{carb}}$ compositions of these samples range from $+3\text{ ‰}$ to $+5\text{ ‰}$, which is relatively heavy and falls within the range of $\delta^{13}\text{C}_{\text{carb}}$ compositions of the rest of the Abadeh-2 section as well as of other studied sections. These findings suggest that the carbon isotope ratios remain close to their primary values. Third, the scatter plot of the $\delta^{13}\text{C}_{\text{carb}}$ and $\delta^{18}\text{O}_{\text{carb}}$ values by facies in each section does not reveal significant and distinct facies-related isotopic patterns except for few samples with unusually light oxygen

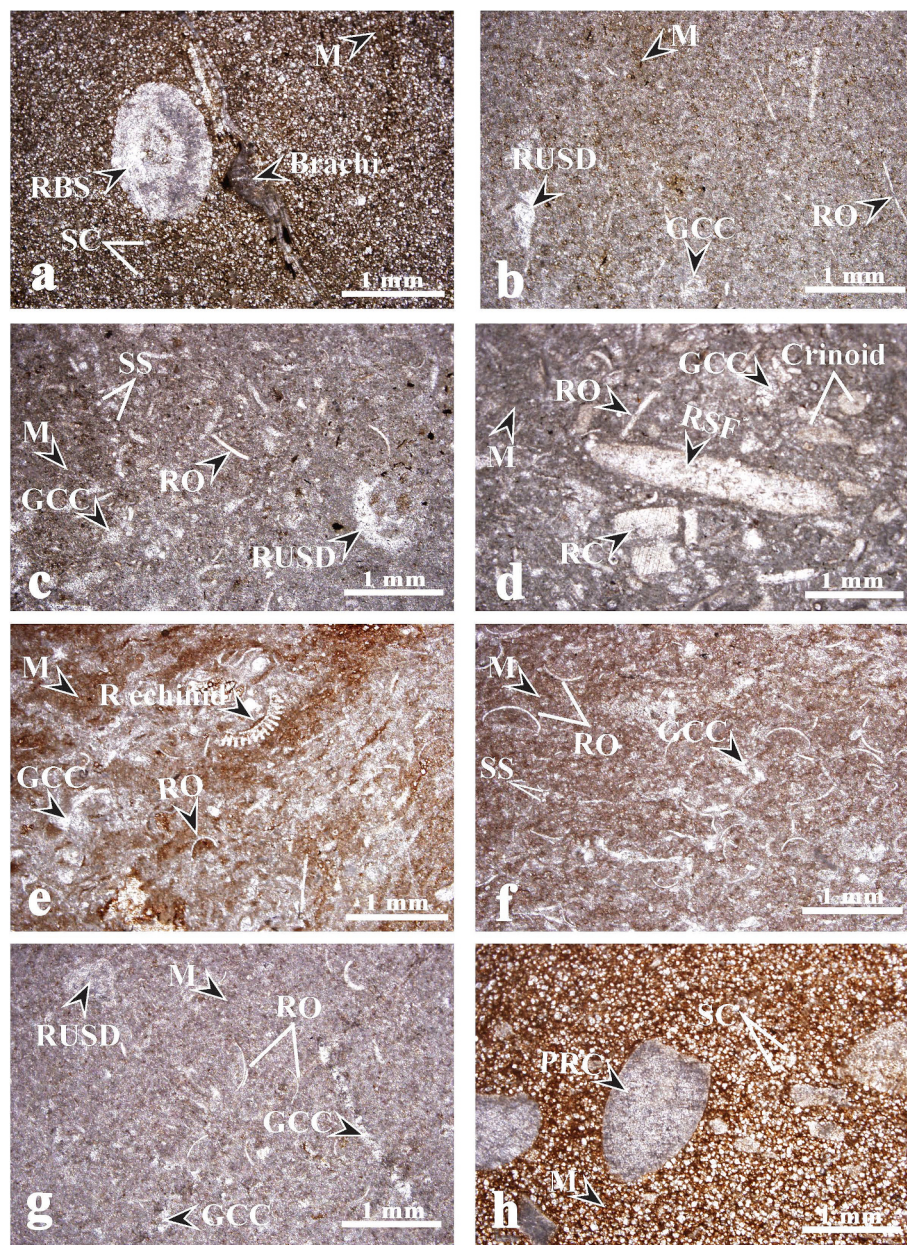


Fig. 9. Photomicrographs of limestone samples from Lower and Upper Julfa and Upper Beds, Ali Bashi and Zal sections, NW Iran. (a) sample J19, recrystallized bioclastic wackestone, Lower Julfa Beds, Ali Bashi section; (b) sample J44, recrystallized bioclastic wackestone, Lower Julfa Beds, Ali Bashi section; (c) sample Z11, recrystallized sponge spicule ostracod wackestone, Lower Julfa Beds, Zal section; (d) sample Z26, recrystallized bioclastic packstone, Lower Julfa Beds, Zal section; (e) sample J54, recrystallized bioclastic wackestone-packstone, Upper Julfa Beds, Ali Bashi section; (f) sample J68, recrystallized ostracod wackestone, Upper Julfa Beds, Ali Bashi section; (g) sample J78, recrystallized ostracod wackestone, Upper Julfa Beds, Ali Bashi section; (h) sample Z59, recrystallized crinoid wackestone, Upper Julfa Beds, Zal section. Abbreviations: Brachi = Brachiopod, RBS = recrystallized brachiopod spine, SC = sparry calcite, M = micrite, RUSD = recrystallized undifferentiated shell debris, GCC = granular calcite cement, RO = recrystallized ostracod, SS = sponge spicule, RSF = recrystallized shell fragment, RC = recrystallized crinoid, R echinid = recrystallized echinid, PRC = partly recrystallized crinoid, F = foraminifer.

and carbon values (Fig. 12). Therefore, we conclude that most samples from study sections preserve nearly primary C-isotope signals. However, future research could productively investigate potential diagenetic alterations in these Iranian sections and comparable sites elsewhere by integrating complementary geochemical proxies, such as Mn/Sr ratios.

6.2. Comparison with previous studies and novel contributions

Although the Ali Bashi, Zal, and Abadeh sections have been previously studied for carbon isotope variations (e.g., Richoz, 2006; Liu et al., 2013; Shen et al., 2013), the dataset presented in this study provides significant advancements in terms of analytical scope, resolution, and

stratigraphic coverage (Fig. 13). Most earlier studies focused exclusively on bulk carbonate carbon isotopes, whereas the present work is the first to integrate both carbonate and organic carbon isotopic data from these Iranian sections. This dual-proxy approach enhances our ability to distinguish between primary environmental signals and secondary diagenetic influences and to more robustly reconstruct carbon cycle dynamics during the Late Permian and the transition into the Triassic. Comparison with the data of Richoz (2006) shows broad agreement in long-term $\delta^{13}\text{C}_{\text{carb}}$ trends, particularly the major shifts near the P-Tr boundary. However, the present study applies significantly higher sampling resolution, which enables the recognition of short-term isotopic fluctuations that are not evident in Richoz's (2006) Wuchiapingian

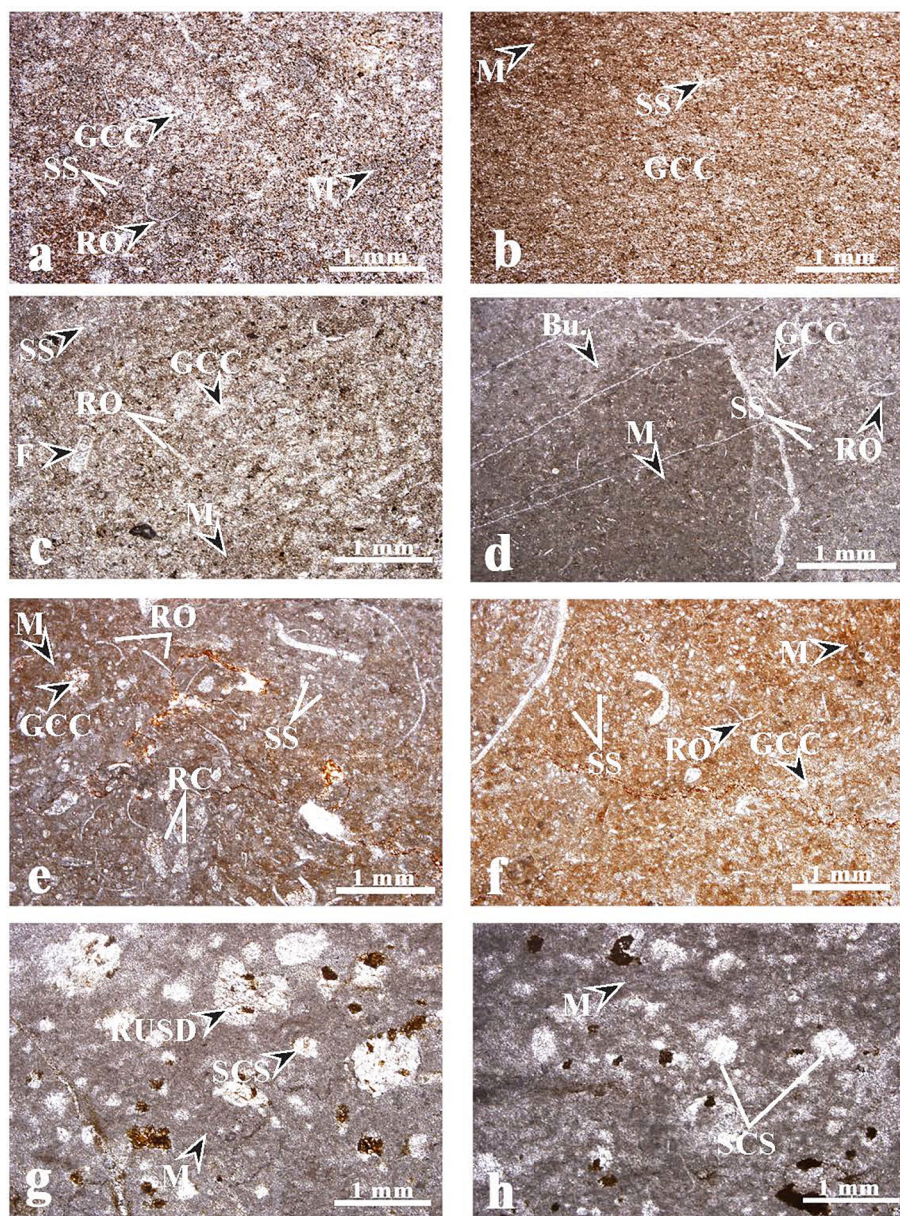


Fig. 10. Photomicrographs of limestone samples from Zal Member, *Paratirolites* Limestone and Elika Formation, Ali Bashi and Zal sections, NW Iran. (a) sample JL92, recrystallized sponge spicule ostracod wackestone, Zal Member, Ali Bashi section; (b) sample JL102, recrystallized mudstone, Zal Member, Ali Bashi section; (c) sample ZS5, recrystallized bioclastic wackestone, Zal Member, Zal section; (d) sample ZS24, recrystallized burrowed ostracod sponge spicule wackestone, Zal Member, Zal section; (e) sample J103, recrystallized bioclastic wackestone, *Paratirolites* Limestone, Ali Bashi section; (f) sample J105, recrystallized bioclastic ostracod sponge spicule wackestone, *Paratirolites* Limestone, Ali Bashi section; (g) sample J116, recrystallized bioclastic wackestone with sparry calcite sphere, Elika Formation, Ali Bashi section; (h) sample ZT10, recrystallized bioclastic wackestone with sparry calcite sphere, Elika Formation, Zal section. Abbreviation: SCS = sparry calcite sphere, for other abbreviations see caption of the Fig. 9.

data from the Ali Bashi and Abadeh sections. These newly resolved variations provide improve the temporal resolution of chemostratigraphic correlations.

A few discrepancies remain between the data from this study and published values from prior studies. Because there is no uniform and consistent offset, we can rule out a calibration issue between labs. Rather, most of these differences appear to result from differences in the facies sampled and perhaps the microsampling approaches within individual hand samples. For example, the carbon isotope data reported by Richoz (2006) from the Changhsingian deposits of the Ali Bashi section are consistently lower than those presented in our study and in Shen et al. (2013). An important consideration is the potential difference in sampled microfacies. Even within the same lithostratigraphic unit, slight variations in depositional facies—such as fine-grained micrite versus

bioclastic or marly carbonates—can influence $\delta^{13}\text{C}$ values due to primary environmental differences or differential susceptibility to diagenesis. In contrast, our study shows that the $\delta^{13}\text{C}$ values from the Upper Permian deposits of the Zal section are systematically lower than those reported by Richoz (2006), especially in the Wuchiapingian interval. This discrepancy likely reflects differences in local paleoenvironmental conditions. The Zal section may have been subject to more restricted marine circulation, varying productivity levels, or water column stratification—all of which could influence the local carbon cycle and result in slightly depleted isotopic values. Furthermore, lithological differences between the sections are a key factor. The Wuchiapingian portion of the Zal section is characterized by mixed carbonate and marl units, which are inherently more susceptible to diagenetic alteration or isotopic dilution due to detrital input. Although we applied careful

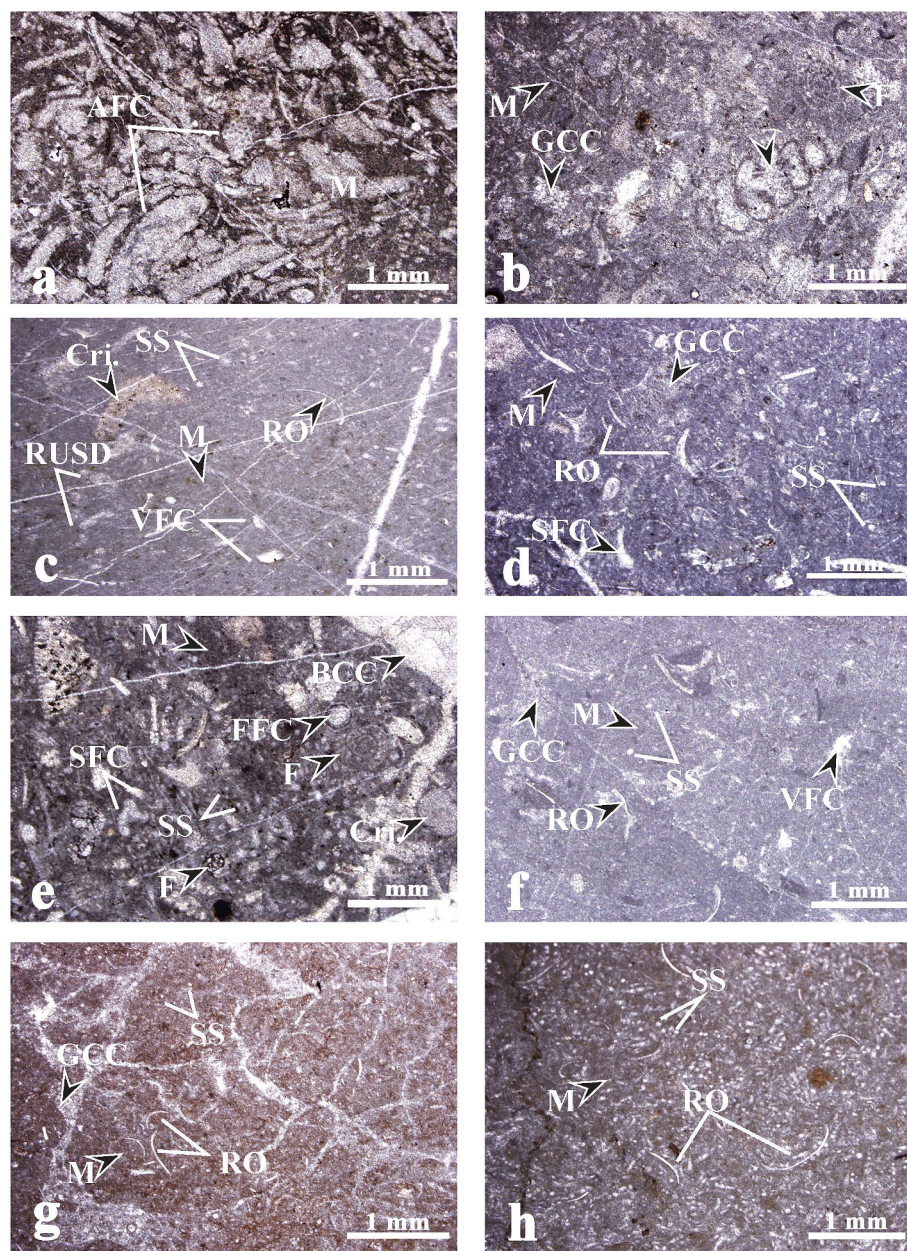


Fig. 11. Photomicrographs of limestone samples from subunit 4b of the Unit 4 and Unit 5 of the Abadeh Formation, units 6 and 7 of the Hambast Formation, Abadeh-1 and Abadeh-2 sections, SW Iran. (a) sample Ab27, recrystallized algal packstone, subunit 4b, Unit 4, Abadeh Formation, Abadeh-1 section; (b) sample Ab64, recrystallized bioclastic wackestone, Unit 5, Abadeh Formation, Abadeh-1 section; (c) sample C22, recrystallized bioclastic wackestone, Unit 6, Hambast Formation, Abadeh-1 section; (d) sample C30, recrystallized bioclastic wackestone, Unit 7, Hambast Formation, Abadeh-1 section; (e) sample H5, recrystallized bioclastic packstone, Unit 5, Abadeh Formation, Abadeh-2 section; (f) sample H18, recrystallized bioclastic wackestone, Unit 6, Hambast Formation, Abadeh-2 section; (g) sample H32, recrystallized bioclastic wackestone, Unit 7, Hambast Formation, Abadeh-2 section; (h) sample H46, recrystallized ostracod sponge wackestone, Unit 7, Hambast Formation, Abadeh-2 section. Abbreviations: AFC = algal fragments filled with calcite, Cri. = Crinoid, FFC = foraminifer filled with calcite, BCC = blocky calcite cement, VFC = void filled with calcite, for other abbreviations see caption of the Fig. 9.

petrographic screening, such effects can be difficult to completely eliminate in bulk carbonate isotope studies. Importantly, the Changsingian values from the Zal section align well with those from Richoz (2006), reinforcing the overall consistency and reliability of our data in a regional context. While the general trends are coherent, the carbon isotope data from the Zal section in our study exhibit more scatter than those reported by Richoz (2006). This variability likely reflects the complex lithological composition of the Zal section, which includes alternations of micritic limestone, shale, and occasional bioclastic beds. Such fine-scale heterogeneity can result in localized fluctuations in $\delta^{13}\text{C}$ values, even among closely spaced samples. Despite careful selection of

well-preserved material and rigorous screening procedures, some degree of micro-scale diagenetic alteration—such as subtle recrystallization or early meteoric influence—may be undetectable through standard petrography but still influence the isotopic signal. In addition, natural environmental variability, including short-term changes in water chemistry or sedimentation rates, can contribute to the observed isotopic scatter. Nevertheless, the overall carbon isotope trend from the Zal section, including the major positive and negative excursions, remains consistent with other Upper Permian datasets from both regional and global records.

Liu et al. (2013) conducted a detailed chemostratigraphic

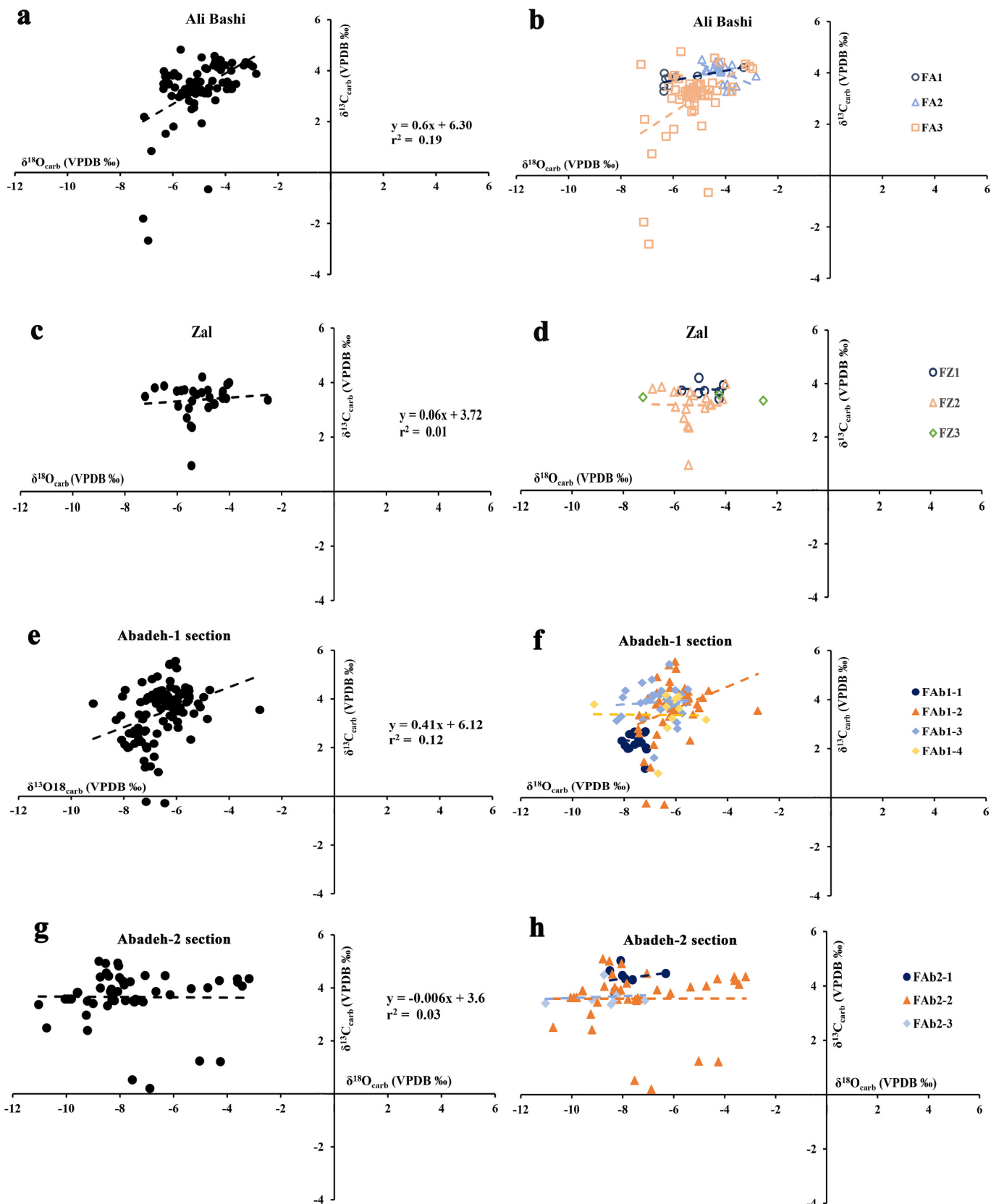


Fig. 12. Cross plots of $\delta^{13}\text{C}$ versus $\delta^{18}\text{O}$ of the Upper Permian bulk carbonates for: (a) and (b) the Ali Bashi section, (b) and (c) the Zal section, (c) and (d) the Abadeh-1 section, (e) and (f) the Abadeh-2 section. The correlation between $\delta^{13}\text{C}$ and $\delta^{18}\text{O}$ is strongest in the Ali Bashi section and Abadeh-1 section. The covariance between $\delta^{13}\text{C}$ versus $\delta^{18}\text{O}$ is really low in Zal section ($r^2 = 0.01$) and Abadeh-2 section ($r^2 = 0.0001$). Considering facies type, the relationship between $\delta^{13}\text{C}$ and $\delta^{18}\text{O}$ does not reveal a distinct pattern between Abadeh-1 section and Abadeh-2 section.

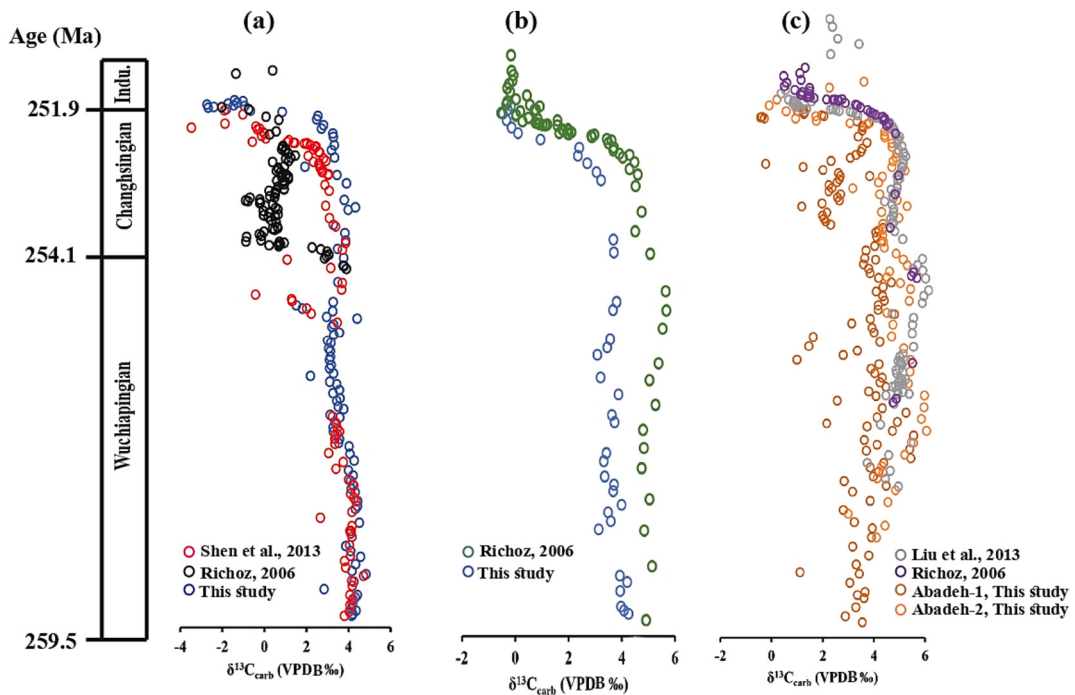


Fig. 13. Comparison of carbon isotope profiles from the Upper Permian to lowermost Triassic intervals in four key stratigraphic sections in Iran including Ali Bashi and Zal in the Julfa region, NW Iran, and Abadeh-1 and Abadeh-2 in the Abadeh region, SW Iran with previously studies. (a) Carbon isotope profile of Ali Bashi section, (b) Carbon isotope profile of Zal section and (c) Carbon isotope profile for Abadeh section. These comparisons illustrate both the consistencies and differences in $\delta^{13}\text{C}$ trends between this study and earlier datasets, demonstrating enhanced stratigraphic resolution and finer-scale isotopic variability captured in this work, particularly across the W-Ch boundary, especially in Ali Bashi and Abadeh sections. This underscores the improved capacity of the present dataset to resolve carbon cycle dynamics leading up to the EPME.

investigation of the Abadeh section in central Iran, focusing on carbon isotope excursions and strontium isotopic compositions ($^{87}\text{Sr}/^{86}\text{Sr}$) to identify and refine the positions of three key chronostratigraphic boundaries: the Guadalupian-Lopingian boundary (GLB), the W-Ch, and the P-Tr boundary (PTEB). Their work provided valuable chemostratigraphic constraints and enhanced the chronostratigraphic resolution of the Lopingian strata at Abadeh. However, their dataset was based exclusively on bulk carbonate carbon isotopes, and the focus of their study was primarily on boundary definitions using combined $\delta^{13}\text{C}_{\text{carb}}$ and $^{87}\text{Sr}/^{86}\text{Sr}$ signatures, rather than a detailed reconstruction of the full carbon cycle dynamics or high-resolution lateral comparisons within the basin. In contrast, the present study provides a more comprehensive geochemical framework by integrating both carbonate and organic carbon isotopic records ($\delta^{13}\text{C}_{\text{carb}}$ and $\delta^{13}\text{C}_{\text{org}}$) from two distinct sections within the Abadeh area: Abadeh-1 and Abadeh-2. This dual-isotope approach enables a more detailed understanding of carbon cycle behavior, as it improves the ability to differentiate between primary signals driven by global carbon cycle perturbations and potential diagenetic overprints or local environmental effects. Furthermore, the addition of $\delta^{13}\text{C}_{\text{org}}$ data adds an important organic-matter perspective that is entirely absent in Liu et al. (2013). Our data also increase the sampling resolution within key intervals, such as the W-Ch boundary, thereby resolving finer-scale isotopic variability that may be critical for understanding pre-extinction environmental instability. The carbon isotope variations across the W-Ch boundary are not distinct or sharply expressed in all studied sections. In the Abadeh section-1 and at Ali Bashi, a minor negative shift apparently occurs and appears in our dataset. However, we believe this shift may reflect local anomalies or outliers rather than a broader, regionally consistent signal. Although the W-Ch boundary is associated with a significant negative $\delta^{13}\text{C}$ excursion in South China sections such as Shangsi and Meishan (Shen et al., 2013), this signal is not clearly expressed in our study sections, likely due to low sedimentation rates, stratigraphic condensation, and post-depositional

diagenetic diffusion typical of deep-marine carbonate settings. Such conditions can smooth out short-term geochemical perturbations and obscure the expression of transient carbon cycle events.

By incorporating two separate sections from Abadeh and juxtaposing our data with published records, we provide new insights into spatial variability in isotopic signals within the same basin, an aspect not addressed in Liu et al. (2013). The $\delta^{13}\text{C}_{\text{carb}}$ dataset from the Ali Bashi section presented in this study also provides a valuable comparison with the high-resolution chemostratigraphic framework of Shen et al. (2013). The novelty of the present study lies in its integration of new $\delta^{13}\text{C}_{\text{org}}$ data alongside $\delta^{13}\text{C}_{\text{carb}}$ from the same stratigraphic sections, which allows for a more detailed assessment of isotopic integrity and environmental versus diagenetic influences. Moreover, while Shen et al. (2013) emphasized global correlation and event stratigraphy, this study focuses on high-resolution reconstruction of regional carbon cycle evolution, which helps bridge local geochemical expressions with global environmental changes.

In summary, this study contributes novel insights into the carbon cycle evolution during the latest Permian by presenting the most detailed $\delta^{13}\text{C}_{\text{carb}}$ and $\delta^{13}\text{C}_{\text{org}}$ records to date from the Ali Bashi, Zal, and Abadeh sections. The combination of expanded spatial coverage, improved sampling density, and dual-isotope analysis distinguishes this work from earlier studies and offers a more detailed understanding of regional carbon cycle responses leading up to the EPME.

6.3. $\delta^{13}\text{C}_{\text{carb}}$, $\delta^{13}\text{C}_{\text{org}}$ and $\Delta^{13}\text{C}$ profiles

One of the tools to assess carbon cycle dynamics is the comparison of $\delta^{13}\text{C}$ variation between marine carbonates and organic matter. In the Iranian sections, the commencement of the $\delta^{13}\text{C}_{\text{carb}}$ and $\delta^{13}\text{C}_{\text{org}}$ changes below the extinction horizon are not contemporaneous (Figs. 4–7). The small decrease of $\delta^{13}\text{C}_{\text{org}}$ in both the Ali Bashi and Zal sections starts before the extinction level from the upper part of the Changhsingian Zal

Member in the Ali Bashi section and from the *Paratirolites* Limestone in the Zal section, with its minimum in the uppermost Changhsingian boundary clay followed by slightly positive excursion in the basal part of the Lower Triassic Elika Formation (Figs. 4 and 5). In the Abadeh-3 section, $\delta^{13}\text{C}_{\text{org}}$ starts with a positive excursion.

from the upper part of the Changhsingian Unit 7 of the Hambast Formation. There are no $\delta^{13}\text{C}_{\text{org}}$ data for the boundary clay, but $\delta^{13}\text{C}_{\text{org}}$ values reach a minimum of -28‰ in the lowermost Triassic microbial buildups (Korte et al., 2004a). Although the trends in $\delta^{13}\text{C}_{\text{carb}}$ and $\delta^{13}\text{C}_{\text{org}}$ begin before the extinction horizon, they do not follow parallel trajectories as would be expected if they recorded the isotope composition of the global surface reservoir in a simple way. For example, in the Julfa sections the decrease in $\delta^{13}\text{C}_{\text{org}}$ starts earlier than the decrease in $\delta^{13}\text{C}_{\text{carb}}$, which is the same in the Abadeh-3 section within the upper Changhsingian Unit 7 (Korte et al., 2004a). Other examples of timing differences in the start of decreasing trends in organic and inorganic carbon isotope records come from the Meishan and Shangsi sections, South China (Riccardi et al., 2007).

Based on data from this study, in the Ali Bashi, Zal, and Abadeh-3 sections, the decreases in $\delta^{13}\text{C}_{\text{carb}}$ and $\delta^{13}\text{C}_{\text{org}}$ start in the upper Changhsingian and continue across the P-Tr boundary. Because the negative excursion in $\delta^{13}\text{C}_{\text{carb}}$ is larger than that in $\delta^{13}\text{C}_{\text{org}}$, there is a decrease in $\Delta^{13}\text{C}$ as well (Figs. 4–5). The low TOC contents in Changhsingian and P-Tr boundary strata in Iran verifies either the low organic productivity or bottom-water oxygenation or both factors (Heydari et al., 2000, 2003; Korte et al., 2004a).

6.4. Global Lopingian signal of the $\delta^{13}\text{C}$

The P-Tr $\delta^{13}\text{C}$ profile has been intensively studied around the world to assess the role of global carbon cycle dynamics in the EPME. Here, we have used the carbon isotope values in well-studied Upper Permian deep-water deposits to improve documentation of the Upper Permian

carbon isotope record prior to the mass extinction event and to examine whether the recorded carbon isotopic changes are reproducible across the Paleo-Tethys and potentially indicative of global carbon cycle dynamics.

6.4.1. Reproducibility patterns of the $\delta^{13}\text{C}_{\text{carb}}$ across the space

Comparison of the Upper Permian $\delta^{13}\text{C}_{\text{carb}}$ records among stratigraphic sections of South China and Iran shows that most sections exhibit relatively heavy and stable to very slightly declining values through the Wuchiapingian and most of the Changhsingian (Fig. 14–16, Fig. S5). The carbonate carbon isotope records of the Chaotian and Shangsi sections are distinct in exhibiting broad negative excursions to values as light as -4‰ within the Wuchiapingian and lower Changhsingian. There is no evidence of such excursions in the other sections from China or Iran, suggesting that these negative shifts at Chaotian and Shangsi are related to local factors. Several factors can cause the carbon isotope composition of primary carbonate sediments to vary over space and time including, for example, local gradients related to net photosynthesis or respiration, ocean circulation patterns, vital effects from calcifying organisms, carbonate mineralogy, and water temperature, among others (Hayes, 1993; Kump and Arthur, 1999; Hay, 2008; Saltzman and Thomas, 2012; Bogumil et al., 2024). Therefore, the reasons behind the differences between the carbon isotope trends of Chaotian and Shangsi sections with Iranian sections could relate to numerous primary factors instead of or in addition to diagenetic alteration.

The $\delta^{13}\text{C}_{\text{carb}}$ records are, if anything, even more consistent across space in the upper Changhsingian and across the P-Tr boundary in both Iran and South China. Every section shows the same trend of the negative carbon excursion starting from mid Changhsingian and continuing across P-Tr boundary. However, the magnitude of the $\delta^{13}\text{C}_{\text{carb}}$ decrease among stratigraphic sections and the lowest values observed vary among sections, from a nadir of $+1\text{‰}$ at the Abadeh-1 section to -2‰

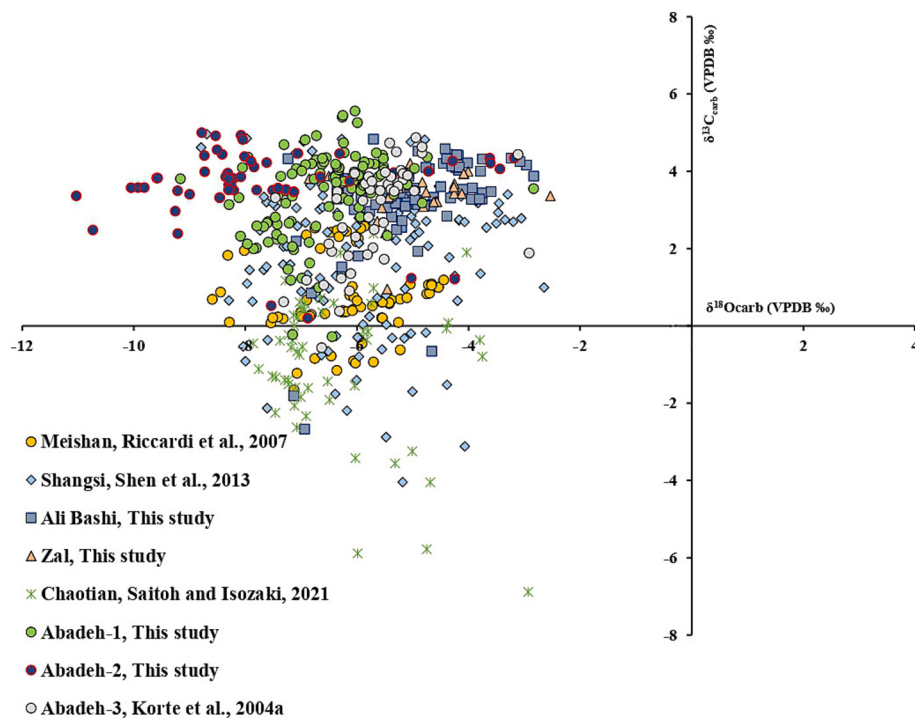


Fig. 14. Late Permian $\delta^{13}\text{C}_{\text{carb}}$ and $\delta^{18}\text{O}_{\text{carb}}$ in deep water studied sections in comparison with literature data (Korte et al., 2004a; Riccardi et al., 2007; Shen et al., 2013; Schobben et al., 2014, 2016; Saitoh and Isozaki, 2021). Two deep water sections, Chaotian and Shangsi, show wider distribution of $\delta^{13}\text{C}_{\text{carb}}$ and narrow distribution of $\delta^{18}\text{O}_{\text{carb}}$ indicative of a diagenetic trend such as oxidation of organic material producing isotopically light carbon. The other sections display moderately lighter $\delta^{13}\text{C}_{\text{carb}}$ but noticeably lighter $\delta^{18}\text{O}_{\text{carb}}$ which suggests either burial diagenesis or meteoric diagenesis where oxygen isotope composition trends to be fluid buffered.

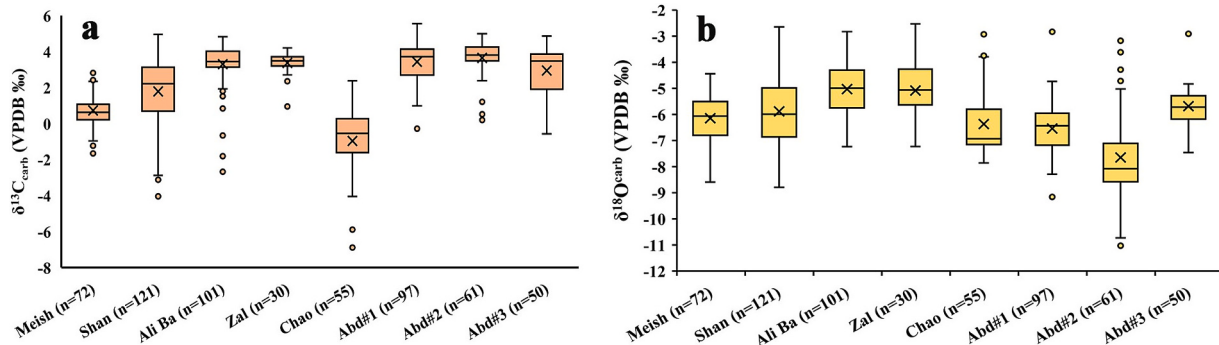


Fig. 15. Box-and-whisker plots showing the range of $\delta^{13}\text{C}_{\text{carb}}$ and $\delta^{18}\text{O}_{\text{carb}}$ values among Upper Permian deep-water sections, illustrating the unusual $\delta^{13}\text{C}_{\text{carb}}$ distributions for Chaotian section (Saitoh and Isozaki, 2021) and unusual light $\delta^{18}\text{O}_{\text{carb}}$ range for Abadeh-2 section. Box plots show maximum size, minimum size, 25th, 50th and 75th percentiles. “n” indicates the number of samples analyzed for carbon and oxygen isotopes compositions in each stratigraphic section. Abbreviations: Meish = Meishan, Shan = Shangsi, Chao = Chaotian, Abd = Abadeh, Ali Ba = Ali Bashi.

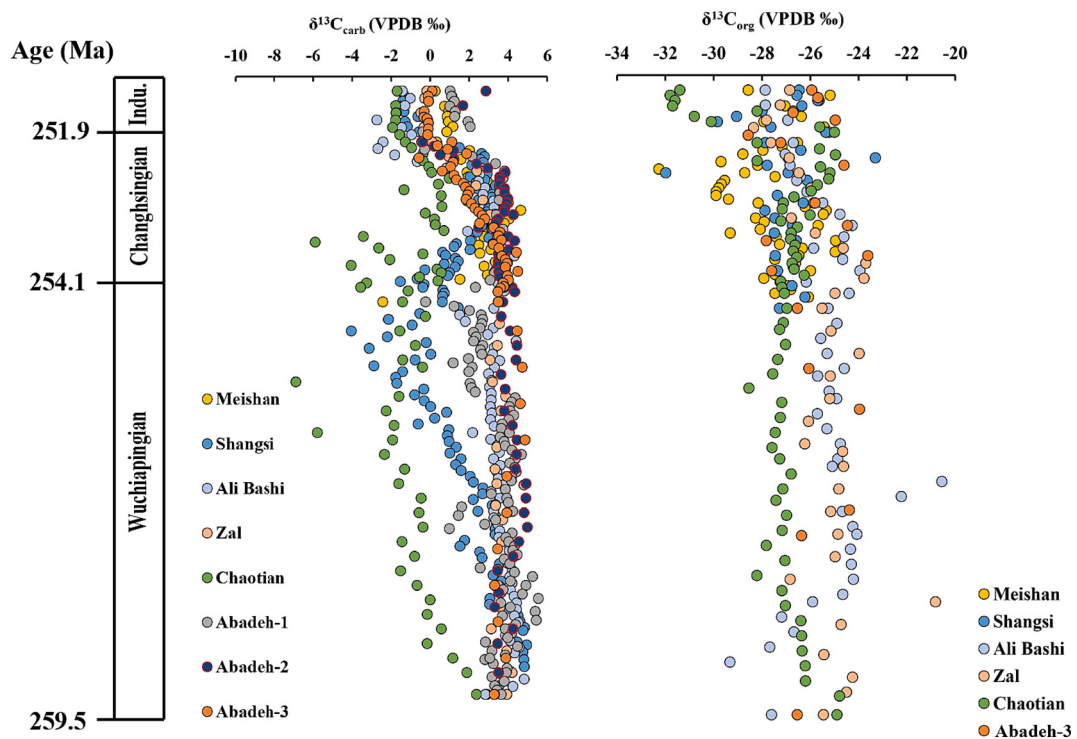


Fig. 16. Lopingian $\delta^{13}\text{C}_{\text{carb}}$ and $\delta^{13}\text{C}_{\text{org}}$ chemostratigraphy and global correlation, illustrating a non-comparable trend between isotopic values of marine carbonates and organic matter. Data sources, for $\delta^{13}\text{C}_{\text{carb}}$ profiles, Meishan from Riccardi et al. (2007), Shangsi from Shen et al. (2013), Chaotian from Saitoh and Isozaki (2021), Abadeh-3 section from Korte et al. (2004a), Ali Bashi, Zal, Abadeh-1 and Abadeh-2 sections from this study; for $\delta^{13}\text{C}_{\text{org}}$ profiles, Meishan and Shangsi from Riccardi et al. (2007), Abadeh from Korte et al. (2004a), Ali Bashi and Zal from this study.

at the Chaotian section.

The size of these spatial gradients is consistent with observed depth gradients in $\delta^{13}\text{C}_{\text{carb}}$ near the P-Tr boundary and within the Lower Triassic in well-preserved shallow-to-deep water transects in South China (Meyer et al., 2011; Song et al., 2013). There is also variation in the magnitude of the reported excursion at the radiometrically and biostatigraphically well-dated Meishan section, where the magnitude of the negative shift varies from 3 ‰ to 8.5 ‰ among studies, though some of the lightest values appear to be outliers (see Saitoh and Isozaki, 2021, for reviews and references).

The stratigraphic consistency of the negative excursions, the correlation of absolute $\delta^{13}\text{C}_{\text{carb}}$ values with depositional facies, and the lack of evidence for meteoric diagenesis as the underlying cause suggest a potential role for respiration of organic matter at the seafloor or in shallow pore waters as a source of isotopically light carbon in several sections,

especially in deeper and more anoxic facies. Because aerobic respiration produces carbon dioxide, locally increasing dissolved inorganic carbon concentrations without adding alkalinity whereas many anaerobic respiration pathways, such as sulfate reduction, iron reduction, and methanogenesis, yield substantial increases in alkalinity, one would expect respiration to be coupled to the local precipitation of carbonate sediment or cements preferentially in settings with oxygen-depleted bottom waters (Higgins et al., 2009; Bergmann et al., 2013),

A further test for the extent to which stratigraphic variation in $\delta^{13}\text{C}_{\text{carb}}$ is globally representative comes from comparison with $\delta^{13}\text{C}_{\text{org}}$ records. In existing data (Fig. 16), the $\delta^{13}\text{C}_{\text{carb}}$ variations are not paralleled in the $\delta^{13}\text{C}_{\text{org}}$ record. Organic carbon isotope values at

Chaotian are systematically lighter than those from other sections, but they do not show the same broad negative excursion that occurs in the $\delta^{13}\text{C}_{\text{carb}}$ record at the same site (Fig. 16). In addition, the $\delta^{13}\text{C}_{\text{org}}$

records lack strong evidence for a sharp negative excursion in $\delta^{13}\text{C}_{\text{org}}$ around the P-Tr boundary (Fig. 16), although prior compilations spanning a greater number of regions and stratigraphic sections have generally supported the existence of such an excursion (Korte and Kozur, 2010). Overall, the $\delta^{13}\text{C}_{\text{org}}$ trend shows carbon cycle stability during the Wuchiapingian and most of the Changhsingian in the Iranian sections, consistent with most of the carbonate records. However, the $\delta^{13}\text{C}_{\text{org}}$ profiles for the upper Changhsingian and P-Tr boundary interval are less coherent among sections (Fig. 16). While the bulk of the evidence continues to support a carbon cycle perturbation beginning in the uppermost Changhsingian, accelerating during the extinction interval and continuing into the lowermost Triassic, there is not strong support for earlier carbon cycle perturbations within the Upper Permian. Assessment of the potential effects from variation in sources of organic carbon as well as potential effects of changing pCO_2 on the isotope fractionation associated with photosynthesis are beyond the scope of currently available data but is likely required for any satisfactory interpretation of these records in terms of global carbon cycle dynamics.

7. Conclusion

Here we report detailed marine $\delta^{13}\text{C}_{\text{carb}}$ and $\delta^{13}\text{C}_{\text{org}}$ in Upper Permian and lowermost Triassic deposits from the Ali Bashi and Zal sections in Julfa area, NW Iran and the Abadeh-1 and Abadeh-2 sections in Hambast Valley, as well as using data from one previously studied section by Korte et al. (2004a) in the Abadeh area, here referred to as the Abadeh-3 section. We have also compared the results of this study with carbon-isotope data from well-studied sections from deeper-water settings in south China spanning the P-Tr boundary to obtain better understanding of which trends in the data are likely to reflect global carbon cycle dynamics.

Petrographic and geochemical indicators of diagenetic alteration show that samples from the studied sections are likely to preserve near-primary C-isotope values in many cases and are, therefore, reliable recorders of local conditions during deposition, meaning that globally reproducible trends from these data may reflect carbon cycle behavior. The isotope records of the studied sections have heavier $\delta^{13}\text{C}_{\text{carb}}$ values than those observed in the Meishan, Shangsi, and Chaotian sections in China, which might result from better preservation of primary carbon-isotope ratios in the Iranian sections as well as moderate spatial gradients in the carbon isotope composition of seawater. The Upper Permian records generally support a stable carbon cycle from the start of the Wuchiapingian through at least the mid-Changhsingian. There is a negative shift in both carbonate and organic matter carbon isotope compositions in Iranian sections below the P-Tr boundary that reaches its minimum at the extinction interval. There are discrepancies between the $\delta^{13}\text{C}_{\text{carb}}$ and $\delta^{13}\text{C}_{\text{org}}$ profiles in the timing of onset of the negative shift before P-Tr boundary and in the magnitude of the negative excursion that highlight the need for continued dissection of the $\delta^{13}\text{C}_{\text{carb}}$ and $\delta^{13}\text{C}_{\text{org}}$ records incorporating information from depositional facies, sample-level petrography, and determination of organic matter sources. Overall, the development of high-resolution carbon isotope records from multiple, widely distributed sites continues to clarify the local versus global components of Permian-Triassic carbon-isotope records.

CRediT authorship contribution statement

Sakineh Arefifard: Writing – original draft. **Christoph Korte:** Writing – review & editing. **Jonathan L. Payne:** Writing – review & editing.

Declaration of competing interest

The authors declare that they have no known competing financial interests or personal relationships that could have appeared to influence the work reported in this paper.

Acknowledgement

We acknowledge B. Petersen (IGN) for sample treatment and carbon isotope analyses. We wish to thank anonymous reviewers for constructive remarks and criticisms during the review process. The first author received financial support from Lorestan University, Iran, for this research under grant number 14014038391403.

Appendix A. Supplementary data

Supplementary data to this article can be found online at <https://doi.org/10.1016/j.palaeo.2025.113268>.

Data availability

Data will be made available on request.

References

- Aghanabati, A., 2004. Geology of Iran. Geological Survey of Iran, p. 586.
- Alavi, M., 1991. Tectonic map of the Middle East, Geological survey of Iran. Scale 1, 500000.
- Alavi, M., 1996. Tectonostratigraphic synthesis and structural style of the Alborz Mountain system in northern Iran. *J. Geodyn.* 21 (1), 1–33.
- Algeo, T.J., Hannigan, R., Rowe, H., Brookfield, M., Baud, A., Krystyn, L., Ellwood, B.B., 2007. Sequencing events across the Permian-Triassic boundary, Guryul Ravine (Kashmir, India). *Palaeogeogr. Palaeoclimatol. Palaeoecol.* 252, 328–346.
- Algeo, T., Henderson, C., Ellwood, B., Rowe, H., Elswick, E., Bates, S., Lyons, T., Hower, J.C., Smith, C., Maynard, J.B., Hays, L., Summons, R., Fulton, J., Freeman, K., 2012. Evidence for a diachronous late Permian marine crisis from the Canadian Arctic region. *Geol. Soc. Am. Bull.* 124 (9–10), 1424–1448.
- Arefifard, S., Baud, A., 2022. Depositional environment and sequence stratigraphy architecture of continuous Upper Permian and Lowermost Triassic deep marine deposits in NW and SW Iran. *Palaeogeogr. Palaeoclimatol. Palaeoecol.* 603, 111187.
- Arefifard, S., Payne, J.L., 2020. End-Guadalupian extinction of larger fusulines in Central Iran and implications for the global biotic crisis. *Palaeogeogr. Palaeoclimatol. Palaeoecol.* 550, 109743.
- Arefifard, S., Payne, J.L., Rizzi, M., 2022. Middle Permian carbon isotope stratigraphy indicates extended interval of carbon cycle stability. *Am. J. Sci.* 322, 1019–1046.
- Baghbani, D., 1993. The Permian Sequence in the Abadeh Region, Central Iran. In: Koroteev, A.V. (Ed.), Contributions to Eurasian Geology. Occasional Publication of Earth Sciences Research Institute, University of South Carolina, pp. 7–22. N.S. 9B.
- Baud, A., Magaritz, M., Holser, W.T., 1989. Permian-Triassic of the Tethys: carbon isotope studies. *Geol. Rundsch.* 78, 649–677.
- Baud, A., Atudorei, V., Sharp, Z., 1996. Late Permian and early Triassic evolution of the Northern Indian margin: carbon isotope and sequence stratigraphy. *Geodin. Acta* 9, 57–77.
- Baud, A., Richoz, S., Brandner, R., Krystyn, L., Heindel, K., Mohtat, T., Mohtat-Aghai, P., Horacek, M., 2021. Sponge takeover from End-Permian Mass Extinction to early Indian Time: Records in Central Iran Microbial Buildups. *Front. Earth Sci.* 9, 1–23.
- Bergmann, K.D., Grotzinger, J.P., Fischer, W.W., 2013. Biological influences on seafloor carbonate precipitation. *Palaios* 28 (2), 99–115.
- Bernasconi, S.M., Meier, I., Wohlwend, S., Brack, P., Hochuli, P.A., Bläsi, H., Wortmann, U.G., Ramseyer, K., 2017. An evaporite-based high-resolution sulfur isotope record of late Permian and Triassic seawater sulfate. *Geochim. Cosmochim. Acta* 204, 331–349.
- Brennecke, G.A., Herrmann, A.D., Algeo, T.J., Anbar, A.D., 2011. Rapid expansion of oceanic anoxia immediately before the end-Permian mass extinction. *Proc. Natl. Acad. Sci.* 108 (43), 17631–17634.
- Brookfield, M.E., Stebbins, A.G., Rampino, M.R., Hannigan, R.E., 2018. Significance of carbon, nitrogen and their isotopic changes in a Permian-Triassic non-marine boundary section at Carlton Heights (Karoo Basin), South Africa. *J. Afr. Earth Sci.* 145, 170–177.
- Brookfield, M.E., Shellnutt, J.G., Yui, T.F., 2022. Climatic fluctuations during a mass extinction: Rapid carbon and oxygen isotope variations across the Permian-Triassic (PTr) boundary at Guryul Ravine, Kashmir, Indi. *J. Asian Earth Sci.* 227, 105066.
- Cao, C.-Q., Wang, W., Jin, Y.-G., 2002. Carbon isotope excursions across the Permian-Triassic boundary in the Meishan section, Zhejiang Province, China. *Chin. Sci. Bull.* 47, 1125–1129.
- Chen, J., Shen, S.-Z., Zhang, Y.-C., Angiolini, L., Gorgij, M.N., Crippa, G., Wang, W., Zhang, H., Yuan, D.-X., Li, X.-H., Xu, Y.-G., 2020. Abrupt warming in the latest Permian detected using highresolution in situ oxygen isotopes of conodont apatite from Abadeh, Central Iran. *Palaeogeogr. Palaeoclimatol. Palaeoecol.* 560, 109973.
- Derry, L.A., Kaufman, A.J., Jacobsen, S.B., 1992. Sedimentary cycling and environmental change in the late Proterozoic: evidence from stable and radiogenic isotopes. *Geochim. Cosmochim. Acta* 56 (3), 1317–1329.
- Elrick, M., Polyak, V., Algeo, T.J., Romaniello, S., Asmerom, Y., Herrmann, A.D., Anbar, A.D., Zhao, L., Chen, Z.Q., 2017. Global-ocean redox variation during the middle-late Permian through early Triassic based on uranium isotope and Th/U trends of marine carbonates. *Geology* 45 (2), 163–166.

- Erwin, D.H., 2006. Extinction: How Life on Earth Nearly Ended 250 Million Years Ago. Princeton University Press, Princeton, NJ, p. 306.
- Friesenbichler, E., Richoz, S., Baud, A., Krystyn, L., Sahakyan, L., Vardanyan, S., Peckmann, J., Reitner, J., Heindel, K., 2018. Sponge-microbial buildups from the lowermost Triassic Chanakhchi section in southern Armenia: microfacies and stable carbon isotopes. *Palaeogeogr. Palaeoclimatol. Palaeoecol.* 490, 653–672.
- Ghaderi, A., Garbelli, C., Angiolini, L., Ashouri, A.R., Korn, D., Rettori, R., Gharai, M.H.M., 2014a. Faunal change near the end-Permian extinction: the brachiopods of the Ali Bashi Mountains, NW Iran. *Riv. Ital. Paleontol. Stratigr.* 120, 27–59.
- Ghaderi, A., Taherpour Khalil Abad, M., Ashouri, A.R., Korn, D., 2016. Permian calcareous algae from the Khachik Formation at the Ali Bashi Mountains, NW of Iran. *Arab. J. Geosci.* 9, 1–11.
- Ghaderi, A., Badpa, M., Ashouri, A.R., 2019. Permian Corals of Ali-Bashi Mountains, Julfa, Northwest of Iran. *Sci. Quarter. J. Geosci.* 29 (114), 97–108.
- Gliwa, J., Ghaderi, A., Leda, L., Schobben, M., Tomás, S., Foster, W.J., Forel, M.B., Ghanizadeh Tabrizi, N., Grasby, S.E., Struck, U., Ashouri, A.R., 2020. Aras Valley (northwest Iran): high-resolution stratigraphy of a continuous central Tethyan Permian-Triassic boundary section. *Fossil Record* 23 (1), 33–69.
- Glaus, M., 1964. Trias und Oberperm im zentralen Elburz (Persien). *Eclogae Geologicae Helvetiae* 57, 497–508.
- Gliwa, J., Forel, M.B., Crasquin, S., Ghaderi, A., Korn, D., 2021. Ostracods from the end-Permian mass extinction in the Aras Valley section (north-West Iran). *Papers in Palaeontology* 7 (2), 1003–1042.
- Gliwa, J., Wiedenbeck, M., Schobben, M., Ullmann, C.V., Kiessling, W., Ghaderi, A., Struck, U., Korn, D., 2022. Gradual warming prior to the end-Permian mass extinction. *Palaeontology* 65 (5), e12621.
- Hassanzadeh, J., Wernicke, B.P., 2016. The Neotethyan Sanandaj-Sirjan zone of Iran as an arche type for passive margin-arc transitions. *Tectonics* 35, 586–621.
- Hemmati, S., Ghaderi, A., Crasquin, S., Ashouri, A.R., 2024. Update and observations on the extraction of ostracods (Crustacea) from the Permian hard carbonate rocks of Iran. *Geodiversitas* 46 (5), 119–133.
- Hermann, E., Hochuli, P.A., Bucher, H., Vigran, J.O., Weissert, H., Bernasconi, S.M., 2010. A close-up view of the Permian-Triassic boundary based on expanded organic carbon isotope records from Norway (Trondelag and Finnmark Platform). *Glob. Planet. Chang.* 74 (3–4), 156–167.
- Heydari, E., Arzani, N., Hassanzadeh, J., 2008. Mantle plume: the invisible serial killer—application to the Permian-Triassic boundary mass extinction. *Palaeogeogr. Palaeoclimatol. Palaeoecol.* 264 (1–2), 147–162.
- Heydari, E., Hassanzadeh, J., Wade, W.J., 2000. Geochemistry of central Tethyan upper Permian and lower Triassic strata, Abadeh region, Iran. *Sediment. Geol.* 137, 85–99.
- Heydari, E., Wade, W.J., Hassanzadeh, J., 2001. Diagenetic origin of carbon and oxygen isotope compositions of Permian-Triassic boundary strata. *Sediment. Geol.* 143 (3–4), 191–197.
- Heydari, E., Hassanzadeh, J., Wade, W.J., Ghazi, A.M., 2003. Permian-Triassic boundary interval in the Abadeh section of Iran with implications for mass extinction: part 1—Sedimentology. *Palaeogeogr. Palaeoclimatol. Palaeoecol.* 193, 405–423.
- Higgins, J.A., Fischer, W.W., Schrag, D.P., 2009. Oxygenation of the ocean and sediments: consequences for the seafloor carbonate factory. *Earth Planet. Sci. Lett.* 284 (1–2), 25–33.
- Holser, W.T., Schönlaub, H.P., Attrep Jr., M., Boeckelmann, K., Klein, P., Magaritz, M., Orth, C.J., Fenninger, A., Jenny, C., Kralik, M., Mauritsch, H., 1989. A unique geochemical record at the Permian/Triassic boundary. *Nature* 337 (6202), 39–44.
- Horacek, M., Richoz, S., Brandner, R., Krystyn, L., Spötl, C., 2007a. Evidence for recurrent changes in lower Triassic oceanic circulation of the Tethys: the $\delta^{13}\text{C}$ record from marine sections in Iran. *Palaeogeogr. Palaeoclimatol. Palaeoecol.* 252, 355–369.
- Horacek, M., Brandner, R., Abart, R., 2007b. Carbon isotope record of the P/T boundary and the lower Triassic in the Southern Alps: evidence for rapid changes in storage of organic carbon. *Palaeogeogr. Palaeoclimatol. Palaeoecol.* 252, 347–354.
- Horacek, M., Koike, T., Richoz, S., 2009. Lower Triassic $\delta^{13}\text{C}$ isotope curve from shallow-marine carbonates in Japan, Panthalassa realm: confirmation of the Tethys $\delta^{13}\text{C}$ curve. *J. Asian Earth Sci.* 36, 481–490.
- Iasa, A., Ghaderi, A., Ashouri, A.R., Korn, D., 2016. Late Permian early Triassic conodonts of the Zal section at the northwest of Iran. *J. Stratigraph. Sedimentol. Res.* 32 (3), 55–74 (in Persian).
- Jin, Y.-G., Wang, Y., Wang, W., Shang, Q.-H., Cao, C.-Q., Erwin, D.H., 2000. Pattern of marine mass extinction near the Permian-Triassic boundary in South China. *Science* 289, 432–436.
- Joachimski, M.M., Lai, X., Shen, S., Jiang, H., Luo, G., Chen, B., Chen, J., Sun, Y., 2012. Climate warming in the latest Permian and the Permian-Triassic mass extinction. *Geology* 40 (3), 195–198.
- Joachimski, M.M., Alekseev, A.S., Grigoryan, A., Gatovsky, Y.A., 2020. Siberian Trap volcanism, global warming and the Permian-Triassic mass extinction: New insights from Armenian Permian-Triassic sections. *GSA Bull.* 132 (1–2), 427–443.
- Jurikova, H., Gutjahr, M., Wallmann, K., Flögel, S., Liebetrau, V., Posenato, R., Angiolini, L., Garbelli, C., Brand, U., Wiedenbeck, M., Eisenhauer, A., 2020. Permian-Triassic mass extinction pulses driven by major marine carbon cycle perturbations. *Nat. Geosci.* 13 (11), 745–750.
- Kaufman, A.J., Knoll, A.H., 1995. Neoproterozoic variations in the C-isotopic composition of seawater: stratigraphic and biogeochemical implications. *Precambrian Res.* 73, 27–49.
- Kaufman, A.J., Jacobsen, S.B., Knoll, A.H., 1993. The Vendian record of Sr and C isotopic variations in seawater: implications for tectonics and paleoclimate. *Earth Planet. Sci. Lett.* 120, 409–430.
- Korn, D., Ghaderi, A., 2019. The Late Permian araxoceratid ammonoids: a case of repetitive temporal and spatial unfolding of homoplastic conch characters. *Neues Jahrbuch für Geologie und Palaontologie—Abhandlungen* 292 (3), 339–350.
- Korn, D., Ghaderi, A., Leda, L., Schobben, M., Ashouri, A.R., 2016. The ammonoids from the late Permian Paratirrolites Limestone of Julfa (East Azerbaijan, Iran). *J. Syst. Palaeontol.* 14, 841–890.
- Korn, D., Leda, L., Heuer, F., Moradi Salimi, H., Farshid, E., Akbari, A., Schobben, M., Ghaderi, A., Struck, U., Gliwa, J., Ware, D., 2021. Baghuk Mountain (Central Iran): high-resolution stratigraphy of a continuous Central Tethyan Permian-Triassic boundary section. *Fossil Record* 24 (1), 171–192.
- Korn, D., Hairapetian, V., Ghaderi, A., Leda, L., Schobben, M., Akbari, A., 2021a. The Changhsingian (late Permian) ammonoids from Baghuk Mountain (Central Iran). *Eur. J. Taxon.* 776, 1–106.
- Korte, C., Kozur, H.W., 2005. Carbon isotope stratigraphy across the Permian/Triassic boundary at Jolfa (NW-Iran), Peitlerkofel (Sas de Putia, Sass de Putia), Pufels (Bula, Bulla), Tesero (all three Southern Alps, Italy) and Gerennavár (Bükk Mts., Hungary). *J. Alpine Geol.* 47, 119–135.
- Korte, C., Kozur, H.W., 2010. Carbon isotope stratigraphy across the Permian-Triassic boundary: A review. *J. Asian Earth Sci.* 39, 215–235.
- Korte, C., Kozur, H.W., Joachimski, M.M., Strauss, H., Veizer, J., Schwark, L., 2004a. Carbon, sulfur, oxygen and strontium isotope records, organic geochemistry and biostratigraphy across the Permian/Triassic boundary in Abadeh, Iran. *Int. J. Earth Sci.* 93, 565–581.
- Korte, C., Kozur, H.W., Mohtat-Aghai, P., 2004b. Dzhulfian to lowermost Triassic $\delta^{13}\text{C}$ record at the Permian/Triassic boundary section at Shahreza, Central Iran. *Hallesches Jahrbuch für Geowissenschaften B Beiheft* 18, 73–78.
- Korte, C., Pande, P., Kalia, P., Kozur, H.W., Joachimski, M.M., Oberhänsli, H., 2010. Massive volcanism at the Permian-Triassic boundary and its impact on the isotopic composition of the ocean and atmosphere. *J. Asian Earth Sci.* 37, 293–311.
- Kozur, H., 1975. Beitrag zur Conodontenfauna des Perm. *Geologische Palaont. Mitteil. Innsbruck* 5 (4), 1–44.
- Kozur, H., 1977. Beiträge zur Stratigraphie des Perm. Teil I: Probleme der Abgrenzung und Gliederung des Perms. *Freiberger Forschungsh C* 319, 79–121.
- Kozur, H.W., 2007. Biostratigraphy and event stratigraphy in Iran around the Permian-Triassic Boundary (PTB): implications for the causes of the PTB biotic crisis. *Glob. Planet. Chang.* 55 (1–3), 155–176.
- Krull, E.S., Lehrmann, D.J., Druke, D., Kessel, B., Yu, Y.-Y., Li, Rong-X., 2004. Stable carbon isotope stratigraphy across the Permian-Triassic boundary in shallow marine carbonate platforms, Nanpanjiang Basin, South China. *Palaeogeogr. Palaeoclimatol. Palaeoecol.* 204, 297–315.
- Lau, K.V., Maher, K., Altiner, D., Kelley, B.M., Kump, L.R., Lehrmann, D.J., Silveira-Tamayo, J.C., Weaver, K.L., Yu, M., Payne, J.L., 2016. Marine anoxia and delayed Earth system recovery after the end-Permian extinction. *Proc. Natl. Acad. Sci.* 113 (9), 2360–2365.
- Leda, L., Korn, D., Ghaderi, A., Hairapetian, V., Struck, U., Reimold, W.U., 2014. Lithostratigraphy and carbonate microfacies across the Permian-Triassic boundary near Julfa (NW Iran) and in the Baghuk Mountains (Central Iran). *Facies* 60, 295–325.
- Li, R., 2017. Petrography and geochemistry of the Permian-Triassic boundary interval, Yangou section, South China: Implications for early Griesbachian seawater $\delta^{13}\text{C}$ DIC gradient with depth. *Sediment. Geol.* 351, 36–47.
- Liu, X.-C., Wang, W., Shen, S.-Z., Gorgij, M.N., Ye, F.-C., Zhang, Y.-C., Furuyama, S., Kano, A., Chen, X.-Z., 2013. Late Guadalupian to Lopingian (Permian) carbon and strontium isotopic chemostratigraphy in the Abadeh section, Central Iran. *Gondwana Res.* 24 (1), 222–232.
- Luo, G., Wang, Y., Algeo, T.J., Kump, L.R., Bai, X., Yang, H., Yao, L., Xie, S., 2011. Enhanced nitrogen fixation in the immediate aftermath of the latest Permian marine mass extinction. *Geology* 39 (7), 647–650.
- Luo, G., Algeo, T.J., Huang, J., Zhou, W., Wang, Y., Yang, H., Richoz, S., Xie, S., 2014. Vertical $\delta^{13}\text{C}_{\text{org}}$ gradients record changes in planktonic microbial community composition during the end-Permian mass extinction. *Palaeogeogr. Palaeoclimatol. Palaeoecol.* 396, 119–131.
- Magaritz, M., Bar, R., Baud, A., Holser, W.T., 1988. The carbon-isotope shift at the Permian/Triassic boundary in the Southern Alps is gradual. *Nature* 331, 337–339.
- Magaritz, M., Krishnamurthy, R.V., Holser, W.T., 1992. Parallel trends in organic and inorganic carbon isotopes across the Permian/Triassic boundary. *Am. J. Sci.* 292, 727–739.
- Meyer, K.M., Yu, M., Jost, A.B., Kelley, B.M., Payne, J.L., 2011. $\delta^{13}\text{C}$ evidence that high primary productivity delayed recovery from end-Permian mass extinction. *Earth Planet. Sci. Lett.* 302, 378–384.
- Musashi, M., Isozaki, Y., Koike, T., Kreulen, R., 2001. Stable carbon isotope signature in mid-Panthalassa shallow-water carbonates across the Permo-Triassic boundary: evidence for ^{13}C -depleted superocean. *Earth Planet. Sci. Lett.* 191, 9–20.
- Nan, J.-Y., Liu, Y.-Y., 2004. Organic and inorganic carbon-isotope shift and paleoenvironment at the P-T boundary section in Meishan, Zhejiang Province. *Geochimica* 33 (1), 9–19 (in Chinese, with English abstract).
- Niko, S., Badpa, M., 2021. Tabulate corals from the Middle and Upper Permian formations in the Julfa area, Northwest Iran. *Bull. National Museum Nat. Sci.* 47, 41–51.
- Payne, J.L., Clapham, M.E., 2012. End-Permian mass extinction in the oceans: an ancient analog for the twenty-first century? *Annu. Rev. Earth Planet. Sci.* 40, 89–111.

- Payne, J.L., Lehrmann, D.J., Wei, Jia-yong, Orchard, M.J., Schrag, D.P., Knoll, A.H., 2004. Large perturbations of the carbon cycle during recovery from the end-Permian extinction. *Science* 305, 506–509.
- Riccardi, A., Kump, L.R., Arthur, M.A., D'Hondt, S., 2007. Carbon isotopic evidence for chemocline upward excursions during the end-Permian event. *Palaeogeogr. Palaeoclimatol. Palaeoecol.* 248, 73–81.
- Richoz, S., 2006. Stratigraphie et variations isotopiques du carbone dans le Permien supérieur et le Trias inférieur de la Neotethys (Turquie, Oman et Iran). *Mémoires de Géologie* (Lausanne) 46, 275p.
- Richoz, S., Krystyn, L., Baud, A., Brandner, R., Horacek, M., Mohtat-Aghai, P., 2010. Permian-Triassic boundary interval in the Middle East (Iran and N. Oman): progressive environmental change from detailed carbonate carbon isotope marine curve and sedimentary evolution. *J. Asian Earth Sci.* 39, 236–253.
- Romano, C., Goudemand, N., Vennemann, T.W., Ware, D., Schneebeli-Hermann, E., Hochuli, P.A., Brühlwiler, T., Brinkmann, W., Bucher, H., 2013. Climatic and biotic upheavals following the end-Permian mass extinction. *Nat. Geosci.* 6, 57–60.
- Saitoh, M., Isozaki, Y., 2021. Carbon isotope chemostratigraphy across the Permian-Triassic boundary at Chaotian, China: implications for the global methane cycle in the aftermath of the extinction. *Front. Earth Sci.* 8, 1–22.
- Sanson-Barrera, A., Hochuli, P.A., Bucher, H., Schneebeli-Hermann, E., Weissert, H., Adatte, T., Bernasconi, S.M., 2015. Late Permian–earliest Triassic high-resolution organic carbon isotope and palynofacies records from Kap Stosch (East Greenland). *Glob. Planet. Chang.* 133, 149–166.
- Schobben, M., Joachimski, M.M., Korn, D., Leda, L., Korte, C., 2014. Palaeotethys seawater temperature rise and an intensified hydrological cycle following the end-Permian mass extinction. *Gondwana Res.* 26 (2), 675–683.
- Schobben, M., Stebbins, A., Ghaderi, A., Strauss, H., Korn, D., Korte, C., 2015. Flourishing Ocean drives the end-Permian marine mass extinction. *Proceed. Nat. Acad. Sci. United States of Am.* 112, 10298–10303.
- Schobben, M., Ullmann, C.V., Leda, L., Korn, D., Struck, U., Reimold, W.U., Ghaderi, A., Algeo, T.J., Korte, C., 2016. Discerning primary versus diagenetic signals in carbonate carbon and oxygen isotope records: an example from the Permian-Triassic boundary of Iran. *Chem. Geol.* 422, 94–107.
- Schobben, M., van de Velde, S., Gliwa, J., Leda, L., Korn, D., Struck, U., Ullmann, C.V., Hairapetian, V., Ghaderi, A., Korte, C., Newton, R.J., Poulton, S.W., Wignall, P.B., 2017. Latest Permian carbonate carbon isotope variability traces heterogeneous organic carbon accumulation and authigenic carbonate formation. *Clim. Past* 13, 1635–1659.
- Schobben, M., Heuer, F., Tietje, M., Ghaderi, A., Korn, D., Korte, C., Wignall, P.B., 2018. Chemostratigraphy across the Permian-Triassic Boundary: the effect of Sampling strategies on Carbonate Carbon Isotope Stratigraphic Markers. In: Sial, A.N., Gaucher, C., Ramkumar, M., Ferreira, V.P. (Eds.), Chemostratigraphy across Major Chronological Boundaries, pp. 159–181.
- Septon, M.A., Veefkind, R.J., Looy, C.V., Visscher, H., Brinkhuis, H., De Leeuw, J.W., 2002. Lateral variations in end-Permian organic matter in northern Italy. In: Buffetaut, E., Koerber, C. (Eds.), Geological and biological effects of impact events, pp. 11–24.
- Seyed-Emami, K., 2003. Triassic in Iran. *Facies* 48, 95–106.
- Shahinfar, S., Yousefi Yeganeh, B., Arefifard, S., Vachard, D., Payne, J.L., 2020. Refined foraminiferal biostratigraphy of upper Wordian, Capitanian and Wuchiapingian strata in Hambast Valley, Abadeh region (Iran), and paleobiogeographic implications. *Geol. J.* 55, 6255–6279.
- Shen, S.-Z., Mei, S.-L., 2010. Lopingian (late Permian) high-resolution conodont biostratigraphy in Iran with comparison to South China zonation. *Geol. J.* 45, 135–161.
- Shen, S.Z., Crowley, J.L., Wang, Y., Bowring, S.A., Erwin, D.H., Sadler, P.M., Cao, C.Q., Rothman, D.H., Henderson, C.M., Ramezani, J., Zhang, H., 2011. Calibrating the end-Permian mass extinction. *Science* 334 (6061), 1367–1372.
- Shen, S.Z., Cao, C.Q., Zhang, H., Bowring, S.A., Henderson, C.M., Payne, J.L., Davydov, V.I., Chen, B., Yuan, D.X., Zhang, Y.C., Wang, W., Zheng, Q.F., 2013. High-resolution $\delta^{13}\text{C}_{\text{carb}}$ chemostratigraphy from latest Guadalupian through earliest Triassic in South China and Iran. *Earth Planet. Sci. Lett.* 375, 156–165.
- Sial, A.N., Chen, J., Korte, C., Pandit, M.K., Spangenberg, J.E., Silva-Tamayo, J.C., Lacerda, L.D.D., Ferreira, V.P., Barbosa, J.A., Gaucher, C., Pereira, N.S., Riedel, P.R., 2021. Hg isotopes and enhanced Hg concentration in the Meishan and Guryul Ravine successions: Proxies for volcanism across the Permian-Triassic boundary. *Front. Earth Sci.* 9, 651224.
- Song, H.Y., Tong, J.N., Algeo, T.J., Horacek, M., Qiu, H.O., Song, H.J., Tian, L., Chen, Z.Q., 2013. Large vertical $\delta^{13}\text{C}$ DIC gradients in early Triassic seas of the South China craton: Implications for oceanographic changes related to Siberian Traps volcanism. *Glob. Planet. Chang.* 105, 7–20.
- Spina, A., Cirilli, S., Sorci, A., Clayton, G., Gennari, V., Ghorbani, M., Ghorbani, M., Ovissi, M., Rettori, G., Rettori, R., 2020. Palynology of the Permian succession from the Ajabshir area (Azerbaijan, Central Iran): a preliminary report. *Geopersia* 10 (1), 211–225.
- Stampfli, G.M., Borel, G.D., 2002. A plate tectonic model for the Paleozoic and Mesozoic constrained by dynamic plate boundaries and restored synthetic oceanic isochrons. *Earth Planet. Sci. Lett.* 196, 17–33.
- Stepanov, D.L., Golshani, F., Stöcklin, J., 1969. Upper Permian and Permian-Triassic Boundary in North Iran. *Geolol. Surv. Iran, Rep.* 12, 1–72.
- Sun, Y., Joachimski, M.M., Wignall, P.B., Yan, C., Chen, Y., Jiang, H., Wang, L., Lai, X., 2012. Lethally hot temperatures during the early Triassic greenhouse. *Science* 338 (6105), 366–370.
- Takahashi, S., Kaiho, K., Oba, M., Kakegawa, T., 2010. A smooth negative shift of organic carbon isotope ratios at an end-Permian mass extinction horizon in central pelagic Panthalassa. *Palaeogeogr. Palaeoclimatol. Palaeoecol.* 292 (3–4), 532–539.
- Taraz, H., Golshani, F., Nakazawa, K., Shimizu, D., Bando, Y., Ishii, K.-I., Murata, M., Okimura, Y., Sakagami, S., Nakamura, K., Tukuoka, T., 1981. The Permian and the lower Triassic systems in Abadeh region, Central Iran. *Mem. Faculty Sci., Kyoto Univers., Series Geol. and Mineral* 47, 62–133.
- Teichert, C., Kummel, B., Sweet, W.C., 1973. Permian-Triassic strata. In: Kuh-e-Ali Bashi, Northwestern Iran, *Bulletin of the Museum of Comparative Zoology*, 145. Harvard University, pp. 359–472.
- Ullmann, C.V., Campbell, H.J., Frei, R., Hesselbo, S.P., Pogge von Strandmann, P.A.E., Korte, C., 2013. Partial diagenetic overprint of late Jurassic belemnites from New Zealand: Implications for the preservation potential of ^87Li values in calcite fossils. *Geochim. Cosmochim. Acta* 120, 80–96.
- Viaretti, M., Crippa, G., Posenato, R., Shen, S., Angiolini, L., 2021. Lopingian brachiopods from the Abadeh section (Central Iran) and their biostratigraphic implications. *Bollettinodella Società Paleontologica Italiana* 60 (3), 213–254.
- Wignall, P.B., Morante, R., Newton, R., 1998. The Permo-Triassic transition in Spitsbergen: $\delta^{13}\text{C}_{\text{org}}$ chemostratigraphy, Fe and S geochemistry, facies, fauna and trace fossils. *Geol. Mag.* 135, 47–62.
- Xu, Dao-qi, Yan, Zheng, 1993. Carbon isotope and iridium event markers near the Permian/Triassic boundary in the Meishan section, Zhejiang province, China. *Palaeogeogr. Palaeoclimatol. Palaeoecol.* 104, 171–176.
- Zakharov, Y.D., Biakov, A.S., Baud, A., Kozur, H., 2005. Significance of Caucasian sections for working out carbon-isotope standard for Upper Permian and lower Triassic (Induan) and their correlation with the Permian of North-Eastern Russia. *J. China Univ. Geosci.* 16, 141–151.
- Zhang, F.F., Romanillo, S.J., Algeo, T.J., Lau, K.V., Clapham, M.E., Richoz, S., Herrmann, A.D., Smith, H., Horacek, M., Anbar, A.D., 2018. Multiple episodes of extensive oceanic anoxia linked to global warming and continental weathering following the latest Permian mass extinction. *Sci. Adv.* 4 (4), e1602921.